

Exploring the Origin of 'Aggregation-Induced Emission' Activity and Mechanofluorochromism in Organometallic Iridium(III) Cationic Complexes: Influence of Counterions

Parvej Alam, Clàudia Climent, Gurpreet Kaur, David Casanova, Angshuman Roy Choudhury, Ashish Gupta, Pere Alemany, and Inamur Rahaman Laskar

Cryst. Growth Des., **Just Accepted Manuscript** • DOI: 10.1021/acs.cgd.6b00810 • Publication Date (Web): 09 Aug 2016

Downloaded from <http://pubs.acs.org> on August 10, 2016

Just Accepted

"Just Accepted" manuscripts have been peer-reviewed and accepted for publication. They are posted online prior to technical editing, formatting for publication and author proofing. The American Chemical Society provides "Just Accepted" as a free service to the research community to expedite the dissemination of scientific material as soon as possible after acceptance. "Just Accepted" manuscripts appear in full in PDF format accompanied by an HTML abstract. "Just Accepted" manuscripts have been fully peer reviewed, but should not be considered the official version of record. They are accessible to all readers and citable by the Digital Object Identifier (DOI®). "Just Accepted" is an optional service offered to authors. Therefore, the "Just Accepted" Web site may not include all articles that will be published in the journal. After a manuscript is technically edited and formatted, it will be removed from the "Just Accepted" Web site and published as an ASAP article. Note that technical editing may introduce minor changes to the manuscript text and/or graphics which could affect content, and all legal disclaimers and ethical guidelines that apply to the journal pertain. ACS cannot be held responsible for errors or consequences arising from the use of information contained in these "Just Accepted" manuscripts.



1
2
3
4
5
6
7 Exploring the Origin of ‘Aggregation Induced
8
9
10
11 Emission’ Activity and ‘Crystallization Induced
12
13
14
15 Emission’ in Organometallic Iridium(III) Cationic
16
17
18
19
20
21
22
23
24
25
26
27
28
29
30
31
32
33
34
35
36
37
38
39
40
41
42
43
44
45
46
47
48
49
50
51
52
53
54
55
56
57
58
59
60

Complexes: Influence of Counterions

Parvej Alam^{a‡}, Clàudia Climent^{b‡}, Gurpreet Kaur^c, David Casanova^{d,e},
Angshuman Roy Choudhury^c, Ashish Gupta^f, Pere Alemany^{*b}, Inamur
Rahaman Laskar^{*a}

^a*Department of Chemistry, Birla Institute of Technology and Science, Pilani, Rajasthan, India.*

^b*Departament de Ciència de Materials i Química Física and Institut de Química Teòrica i Computacional (IQTCUB), Universitat de Barcelona, Martí i Franquès 1-11, Barcelona 08028, Spain.*

^c*Department of Chemical Sciences, Indian Institute of Science Education and Research (IISER), Mohali, Sector 81, S. A. S. Nagar, Manauli PO, Mohali, Punjab, 140306, India.*

^d*Kimika Fakultatea, Euskal Herriko Unibertsitatea (UPV/EHU), Donostia International Physics Center, Paseo Manuel de Lardizabal, 4, Donostia 20018, Spain.*

^e*IKERBASQUE, Basque Foundation for Science, Bilbao 48013, Spain.*

^f*Samtel Center for Display Technologies, IIT Kanpur, Kanpur, (U.P), India†*

‡*Both authors have contributed equally to this work developing the experimental (P.Alam) and computational (C.Climent) parts, respectively.*

KEYWORDS. Iridium(III) complex, Aggregation Induced Emission (AIE), Counterions dependent color, Crystallization Induced Emission, DFT calculations.

ABSTRACT: A new cationic iridium(III) complex exhibiting ‘aggregation induced emission (AIE)’ activity, $[\text{Ir}(\text{PPh}_3)_2(\text{bipy})(\text{H})_2]\text{A}$ (bipy = 2,2'-bipyridine; A = counterions) has been synthesized in a straightforward synthetic route. Interestingly, the emission colour of solid state samples of this complex varied with different counteranions $[\text{A} = \text{Cl}^-, \text{BF}_4^-, \text{PF}_6^-, \text{N}(\text{CN})_2^-]$ and crystallization induced emission was observed. The emission properties for the compounds with $\text{A} = \text{Cl}^-, \text{PF}_6^-$ are discussed by analyzing the crystal packing, the frontier molecular orbitals and the calculation of the relevant low-lying excited states using time dependent density functional theory. The restriction of internal rotation of the phenyl rings in the phosphine ligands due to intermolecular interactions is suggested as the most plausible origin of the observed AIE effect in these crystals.

INTRODUCTION

Smart solid state luminescent materials responsive to external stimuli such as shearing, grinding, rubbing, solvent exposure, or temperature changes have received considerable attention in recent times.¹ The principal interest in these materials stems from their ability to change their emission colour as a response to an external perturbation that triggers changes in the network of weak non-covalent interactions between individual molecules in molecular aggregates.²⁻⁹ These materials have an immense potentiality in various applications such as optical data recorders, mechanical sensors, security paper, deformation detectors or storage devices.¹⁰⁻²¹ In order to enhance the existing capabilities and guide the design of new improved materials, it is, however, necessary to develop a deep understanding of the physical nature of the mechanisms involved in their response to external perturbations.

In the field of luminescent compounds with technological applications, iridium(III) coordination complexes have drawn enormous attention in the last decade, mainly because of their rich excited-state properties.²²⁻²⁶ The presence of strong spin-orbit coupling (SOC) renowned it as one of the most efficient known triplet emitters, resulting in bright phosphorescence observed even at room temperature.²⁷⁻²⁹ Additionally, the long emissive lifetimes, large Stoke shifts, high quantum yields, and the existence of straightforward synthetic routes for the preparation of these compounds has made them specially attractive as novel materials for diverse state-of-the-art technological applications^{30, 31} such as flat-panel displays, lighting systems or cell imaging.³²⁻³⁵

For the ultimate application of these iridium(III) compounds in optoelectronic devices, it is evident that an enhanced emission in the solid state would be highly desirable, so that increasingly improved solid state quantum efficiencies should be obtained.

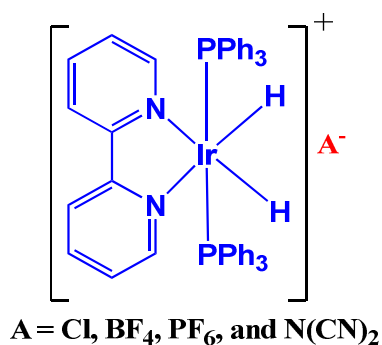
1
2
3 In recent years, the aggregation-induced emission (AIE)³⁶⁻⁴⁶ as well as the enhanced
4 phosphorescence emission in the solid state (EPESS)^{47, 48} terms has been coined to describe this
5 enhancement of the emission in crystalline or aggregated forms as compared to that in dilute
6 solutions. Although from an experimental point of view it is quite straightforward to identify the
7 presence of the AIE effect, in most of the cases, its physical origin still remains unclear. Several
8 alternative mechanisms have been proposed to rationalize its appearance for different families of
9 compounds, including the restriction of intramolecular motions (RIM),^{49, 50} E/Z isomerizations,⁵¹
10 J-aggregate formation,⁵² twisted intramolecular charge transfer (TICT),⁵³ excited-state
11 intramolecular proton transfer (ESIPT),⁵⁴ conformational planarization,⁵⁵ or excimer formation.⁵⁶
12 Although within a short span of time, the number of compounds showing AIE has increased
13 notably, investigations of the detailed mechanism causing this effect are still scarce and some
14 controversy on alternative explanations for the origin of AIE in some compounds can be found in
15 the literature.^{48, 57-61}

16
17
18 Recently, some of us reported⁵⁹ the synthesis of a new AIE active complex of iridium(III),
19 [Ir(PPh₃)₂(bipy-H)(Cl)(H)] or [Ir(bipy-H)] (bipy-H = κ²-N,C-2,2'-bipyridine) obtained by a
20 "rollover" cyclometalation reaction⁶² in which the bipyridine ligand binds to the metal center in a
21 C[^]N mode instead of the usual N[^]N one. For this complex, reversible protonation and
22 deprotonation of the non-coordinated nitrogen atom in the bipyridine ligand is possible, both in
23 solution and in the solid state, leading to a shift in the emission colour that depends on the *pK_a* of
24 the employed acid. In addition to this rare rollover-type complex, a very similar cationic complex
25 [Ir(bipy)H₂(PPh₃)₂]⁺ or [Ir(bipy)]⁺ (**1**) was also obtained with the expected N[^]N coordination
26 mode for the bipyridine ligand. In the present work, we explore the differences in the solid state
27 emission of **1** depending on the nature of the counterions (Cl⁻, N(CN)₂⁻, BF₄⁻ and PF₆⁻) used to
28
29
30
31
32
33
34
35
36
37
38
39
40
41
42
43
44
45
46
47
48
49
50
51
52
53
54
55
56
57
58
59
60

obtain the crystals. Since all the studied solid-state samples for this cationic complex exhibit a more or less pronounced AIE activity regardless of the counterion that they contain, a careful comparison of their crystal structures offers an excellent opportunity to try to shed some light in the effects of the crystal environment and intermolecular interactions on their AIE activity.

One of the complexes was also found to exhibit crystallization induced emission (CIE).^{1, 63-67}

This unusual behavior refers to colour changes of the complex in the solid state when it is put under stress as for instance by mechanical grinding, a phenomenon that can be greatly exploited for several applications.



Scheme 1. Structure of $[\text{Ir}(\text{bipy})\text{H}_2(\text{PPh}_3)_2]\text{A}$

EXPERIMENTAL SECTION

Materials

Iridium(III) chloride hydrate, 2,2'-bipyridine, triphenylphosphine and 2-ethoxyethanol were purchased from the Sigma Aldrich Chemical Company Ltd., while sodium borohydride,

1
2
3 potassium hexafluorophosphate, sodium dicyanamide, as well as all spectroscopic grade solvents
4
5 (dichloromethane (DCM), methanol, etc.) were procured from the Merck Company.
6
7

8
9 **Synthesis, characterization, and sample preparation of [Ir(bipy)H₂(PPh₃)₂]A (A⁻ = Cl⁻,
10
11 N(CN)₂⁻, PF₆⁻, BF₄⁻)**
12

13 To a stirred solution of IrCl₃·3H₂O (0.5025 mmol) in 2-ethoxyethanol (6 mL), triphenyl
14 phosphine (1.507 mmol) was added and the reaction mixture refluxed at 130°C for 4h.
15
16 Afterwards, the reaction mixture was basified with an excess of Na₂CO₃ (~10 mmol). Then, 2,2'-
17 bipyridine (1.252 mmol) was added to the reaction mixture which was refluxed further for 3h.
18
19 The resulting reaction mass was cooled to room temperature. The final solid mass contained two
20 products, [Ir(bipy-H)(PPh₃)₂(H)(Cl)] (minor) and [Ir(bipy)H₂(PPh₃)₂]Cl (major), and it was
21 purified by column chromatography. Both products were further recrystallized using a mixture of
22 DCM and hexane (1:1).
23
24
25
26
27
28
29
30
31

32 The ion exchange reaction was carried out in a microwave reactor (MW) and it was completed
33 within a very short period of time. The methanolic solution (2 mL) of [Ir(bipy)H₂(PPh₃)₂]Cl was
34 placed in a microwave tube along with NaBF₄/KPF₆/Na[N(CN)₂] and 2 mL methanol. The whole
35 reaction mixture was heated at 80°C for 5 minutes. After cooling, the solid product was separated
36 out from the reaction mixture and purified by recrystallization with a mixture of
37 methanol/hexane (~70-80%). Single crystals of [Ir(bipy)]Cl and [Ir(bipy)]PF₆ were grown using
38 toluene and hexane/DCM mixture, respectively.
39
40
41
42
43
44
45
46
47
48

49 ¹H, ¹³C and ³¹P NMR spectra were recorded in a 400 MHz Bruker spectrometer using CDCl₃ and
50 DMSO-d₆ as solvents. Tetramethylsilane (TMS, δ = 0 for ¹H and ¹³C NMR) and phosphoric acid
51 (H₃PO₄, δ = 0 for ³¹P NMR) were used as internal standards. UV-VIS absorption spectra in
52 solution state were recorded in a Shimadzu Spectrophotometer (model UV-1800), while
53
54
55
56
57
58
59
60

1
2
3 absorption spectra for thin films were recorded in a Shimadzu Spectrophotometer (model UV
4
5 2550). The steady state photoluminescence spectra were recorded on a FLS920-s Edinburgh
6
7 spectrofluorometer, while the solution state and solid state (thin film) photoluminescence (PL)
8
9 spectra were recorded on Shimadzu (A40195003382SA) and Fluoromax-4 (0406C-0809)
10
11 spectrofluorophotometers, respectively. The solid state quantum yield of the powder samples
12
13 were measured using a calibrated integrating sphere in a Gemini spectrophotometer (Gemini
14
15 180). High-resolution mass spectrometry (HRMS) experiments were carried out with a (TOF MS
16
17 ES+1.38 eV) VG Analytical (70-S) spectrometer and Q-ToF micro mass spectrometer. Infrared
18
19 spectra were recorded using FTIR Shimadzu (IR prestige-21) and Perkin Elmer Spectrum 100
20
21 FTIR spectrometers. Microwave assisted reactions were carried out in a CEM Discover (model
22
23 1908010) reactor. Powder XRD (PXRD) data were measured by using a Rigaku miniflex II
24
25 desktop X-ray diffractometer. All the reactions were performed under nitrogen atmosphere and
26
27 their progress monitored using thin-layer chromatography (TLC) plates (pre-coated with 0.20
28
29 mm silica gel). The whole experiment was conducted under inert atmosphere.

30
31
32 The ^1H NMR signal of the metal-hydride peak appeared in the range of -19.55 to
33
34 -19.46 ppm as a triplet with a spin-spin coupling constant value, $J_{(\text{P-H})} \sim 16.7$ Hz, which
35
36 was in accordance with each of the hydrides lying *cis* to two phosphorus atoms. There
37
38 were no significant differences found in the m/z values of the HRMS spectra for
39
40 complexes $[\text{Ir}(\text{bipy})\text{H}_2(\text{PPh}_3)_2]\text{A}$, where $\text{A} = \text{Cl}, \text{BF}_4, \text{PF}_6$ and $\text{N}(\text{CN})_2$, showing that in all
41
42 four cases the same cationic species was present (Scheme 1). The presence of counterions
43
44 was confirmed by measuring FTIR stretching frequencies. The complex containing the
45
46 PF_6^- counterion was earlier synthesized using $[\text{Ir}(\text{H})_2(\text{PPh}_3)_2(\text{acetone})_2]\text{BF}_4$ as a
47
48 precursor^{68, 69} which showed a strong peak at 840 cm^{-1} ($\nu_{\text{P-F}}$),⁷⁰ the BF_4^- containing
49
50
51
52
53
54
55
56
57
58
59
60

1
2
3 complex a stretching frequency at 1058 cm^{-1} ($\nu_{\text{B-F}}$),⁷¹ while the complex with a $\text{N}(\text{CN})_2^-$
4 counterion showed peaks at 2128 and 2184 cm^{-1} (CN),⁷² respectively.
5
6

7
8 **[Ir(bipy)H₂(PPh₃)₂]Cl:** ¹H NMR (400 MHz, CDCl₃) δ 9.00 (d, $J = 8.5$ Hz, 2H), 7.92 (t, $J = 7.3$
9 Hz, 4H), 7.30 (d, $J = 6.8$ Hz, 5H), 7.28 – 7.19 (m, 23H), 6.64 (dd, $J = 7.2, 5.1$ Hz, 2H), -19.55 (t,
10 $J = 16.9$ Hz, 2H); ³¹P NMR (162 MHz, CDCl₃) δ 19.16; ¹³C NMR (101 MHz, CDCl₃) δ 156.02,
11 154.19, 137.92, 133.13, 133.07, 133.01, 131.64, 131.37, 131.10, 130.21, 128.35, 128.30, 128.25,
12 126.24, 125.72. IR (KBr, cm^{-1}): 2141, 2168 (m, $\nu_{\text{Ir-H}}$); ESI-HRMS, calculated: ($[\text{M}]^+$), m/z
13 875.2296, found: ($[\text{M}]^+$), m/z 875.2355 (Figure S1).
14
15
16
17
18
19
20
21

22 **[Ir(bipy)H₂(PPh₃)₂]N(CN)₂:** ¹H NMR (400 MHz, CDCl₃) δ 8.33 (d, $J = 8.2$ Hz, 1H), 8.03 (d, J
23 = 5.3 Hz, 1H), 7.87 (t, $J = 7.8$ Hz, 1H), 7.40 – 7.17 (m, 14H), 6.75 – 6.67 (m, 1H), -19.51 (t, $J =$
24 16.7 Hz, 1H); ³¹P NMR (162 MHz, CDCl₃) δ 20.52; ¹³C NMR (101 MHz, CDCl₃) δ 155.76,
25 154.52, 137.57, 133.11, 133.05, 132.99, 131.51, 131.24, 130.97, 130.33, 128.43, 128.38, 128.33,
26 126.45, 124.28, 120.31. IR (KBr, cm^{-1}): 2221, 2190 (m, $\nu_{\text{Ir-H}}$), 2128 (s, ν_{CN}), 2184(m, ν_{CN}); ESI-
27 HRMS, calculated: ($[\text{M}]^+$), m/z 875.2296, found: ($[\text{M}]^+$), m/z 875.2355 (Figure S2).
28
29
30
31
32
33
34
35

36 **[Ir(bipy)H₂(PPh₃)₂]PF₆:** ¹H NMR (400 MHz, DMSO) δ 8.33 (d, $J = 5.3$ Hz, 1H), 8.22 (d, $J =$
37 8.2 Hz, 1H), 7.83 (t, $J = 7.4$ Hz, 1H), 7.47 – 7.21 (m, 15H), 7.01 – 6.84 (m, 1H), -19.46 (t, $J =$
38 16.7 Hz, 1H); ³¹P NMR (162 MHz, DMSO) δ 19.17. IR (KBr, cm^{-1}): 2136, 2160 (m, $\nu_{\text{Ir-H}}$) 840 (s,
39 $\nu_{\text{P-F}}$); ESI-HRMS, calculated: ($[\text{M}]^+$), m/z 875.2296, found: ($[\text{M}]^+$), m/z 875.2356 (Figure S3).
40
41
42
43
44
45

46 **[Ir(bipy)H₂(PPh₃)₂]BF₄:** ¹H NMR (400 MHz, DMSO) δ 8.33 (d, $J = 5.3$ Hz, 1H), 8.22 (d, $J =$
47 8.2 Hz, 1H), 7.84 (t, $J = 7.4$ Hz, 1H), 7.42 – 7.20 (m, 14H), 6.98 – 6.89 (m, 1H), -19.46 (t, $J =$
48 16.7 Hz, 1H), ³¹P NMR (162 MHz, DMSO) δ 19.64. IR (KBr, cm^{-1}): 2220, 2150 (m, $\nu_{\text{Ir-H}}$),
49 1058(m, $\nu_{\text{B-F}}$); ESI-HRMS, calculated: ($[\text{M}]^+$), m/z 875.2296, found: ($[\text{M}]^+$), m/z 875.2374
50 (Figure S4).
51
52
53
54
55
56
57
58
59
60

X-ray single crystal diffraction study

Single crystal X-ray diffraction data for $[\text{Ir}(\text{bipy})\text{H}_2(\text{PPh}_3)_2]\text{Cl}$ and $[\text{Ir}(\text{bipy})\text{H}_2(\text{PPh}_3)_2]\text{PF}_6$ were recorded on a Rigaku XtaLAB mini single crystal X-ray diffractometer equipped with a Mercury 375/M CCD detector and graphite monochromated Mo – K_α radiation. The data set was collected at 100.0(1) K by using an Oxford cryosystem. The data were processed using the Rigaku Crystal Clear suite 2.0.⁷³ The crystal structure was solved and refined with SHELXS2013 and SHELXL2013⁷⁴ available within Olex2⁷⁵.

Computational details

Ground state optimizations and frequency calculations were carried out within the framework of density functional theory (DFT) with the B3LYP⁷⁶⁻⁷⁸ hybrid functional in combination with a basis set of double- ζ quality (LANL2DZ) and the effective core potential of Hay and Wadt⁷⁹ for iridium, while the standard 6-31G(d) basis set was used for the rest of atoms in the molecule. Vertical transition energies were calculated using time dependent density functional theory (TD-DFT) with the same exchange-correlation functional and basis sets. The geometry for the lowest excited triplet state was also optimized at the same level of theory.

In order to have a reference structure for the isolated cation, the optimization calculations have been carried out in the vacuum. Since in this study we are only seeking for a qualitative explanation of the experimentally observed trends by comparing the calculations for different geometries of the same cation, we have not considered the necessity of accounting for the effects of solvation on the photophysical properties in solution by including a solvent model in our calculations. A guess of the atomic positions of the two hydrogen atoms coordinating the iridium atom in the $[\text{Ir}(\text{bipy})\text{H}_2(\text{PPh}_3)_2]\text{Cl}$ and $[\text{Ir}(\text{bipy})\text{H}_2(\text{PPh}_3)_2]\text{PF}_6$ crystals has been obtained through restricted geometry optimizations in which all atoms have been frozen in the geometry obtained

1
2
3 from X-ray diffraction and only the two hydrogen atoms were allowed to move in the energy
4 minimization procedure. The basis set used in this calculation was 6-31G(d,p). Throughout the
5 paper, whenever the cation in the crystal's geometry is mentioned, it will correspond to this latter
6 geometry. These restricted optimizations were also carried out in the presence of nearby
7 counterions, but practically the same final positions for the hydrogen atoms were obtained. The
8 ground state and the lowest triplet state of cation **1** were optimized starting from the monomer's
9 geometry in the Ir(bipy)H₂(PPh₃)₂Cl and [Ir(bipy)H₂(PPh₃)₂]PF₆ crystals. The same ground state
10 was obtained starting from either geometry, while for the triplet states some differences in the
11 relative orientations of the phenyl rings of the phosphine ligands were observed. Nevertheless,
12 the pseudooctahedral environment of the iridium atom and the geometry for the bipyridine ligand
13 that determine the energy for the emission band were practically identical in the two geometries
14 for the T₁ state. For this reason, we will refer only to one optimized S₀ and T₁ geometry for the
15 cation throughout the paper. All electronic structure calculations reported in this study were
16 performed with the GAUSSIAN 09 suite of programs.⁷⁶

37 38 **RESULTS AND DISCUSSION**

39 **Molecular and crystal structure**

40
41
42 The principal building block in the synthesized crystals is a cationic iridium(III) complex **1** with
43 a distorted octahedral coordination sphere (Figure 1), as confirmed by the SC-XRD analysis
44 obtained for the [Ir(bipy)]Cl and [Ir(bipy)]PF₆ crystals. A bipyridine ligand along with two
45 hydride ligands lies on the equatorial plane while the axial positions are occupied by two
46 triphenylphosphine ligands. The chiral propeller-like arrangement of the phenyl rings in the
47
48
49
50
51
52
53
54
55
56
57
58
59
60

1
2
3 triphenylphosphine ligand allows the possibility of having enantiomeric molecules. Indeed, the
4
5 two possible enantiomers are present in the two studied crystal structures.
6
7
8
9

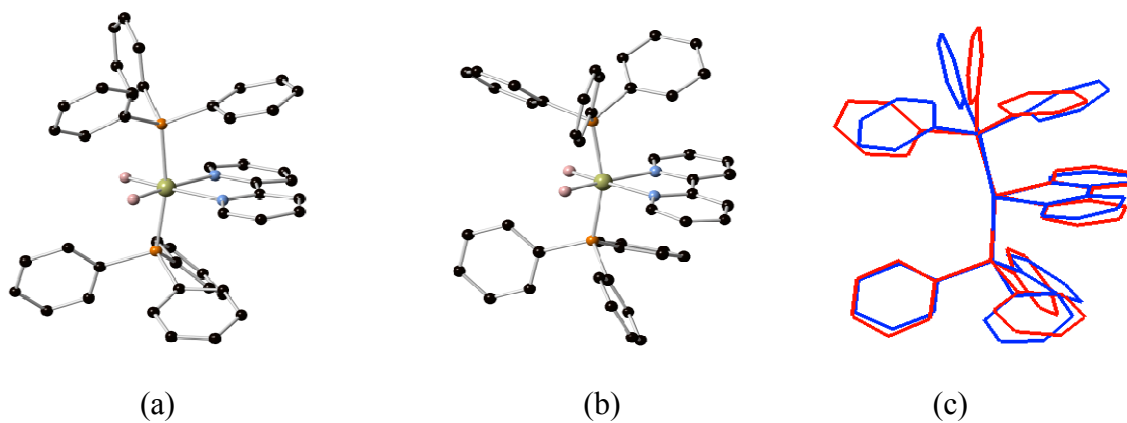


Figure 1. Structures of **1** in the (a) [Ir(bipy)]Cl and (b) [Ir(bipy)]PF₆ crystals with the optimized hydride ligands and (c) the superposition of their most overlapping enantiomers. Hydrogen atoms on the ligands are not shown for the sake of clarity.

Table S1 and S2 contains the principal geometrical parameters of the Ir coordination sphere for the two experimental X-ray diffraction structures, revealing that the two geometries are rather similar. The main departure from a perfect octahedral environment for the iridium atom corresponds to the off-axis distortion of the two phosphorous atoms, with P-Ir-P angles on the side of the two hydride ligands about 15° smaller than in a perfect octahedron (180°). Bond distances between the central metal atom and the coordinating atoms on the ligands are very similar in the two crystal structures, except for one of the Ir-N bonds, which is approximately 0.05 Å longer in the [Ir(bipy)]PF₆ crystal. This is because the bipyridine ligand in both structures has some differences in the adopted geometry, probably due to intermolecular forces induced by

1
2
3 the bulky phenylphosphine ligands. Nevertheless, these differences do not have a great impact on
4 the electronic structure of the cation, as suggested by our calculations discussed below. The
5 major differences between the two geometries essentially correspond to the relative disposition
6 of the phosphine ligands (Figure 1c). In the [Ir(bipy)]PF₆ crystal, the two sets of phenyl rings of
7 the two phosphine groups in *trans* disposition are closer to an eclipsed conformation than in the
8 [Ir(bipy)]Cl case, as indicated by their C-P-P-C dihedral angles (Table S1). In close relation to
9 this distortion, we notice that the molecular geometries for the two crystals exhibit different
10 degrees of rotation for some of the phenyl rings.
11
12
13
14
15
16
17
18
19
20
21

22 In the unit cell of both crystals, there are four cations and four counterions, but the [Ir(bipy)]PF₆
23 crystal contains six additional DCM molecules. The four cations in the unit cell are symmetry
24 equivalent, although in the two crystals they appear as two pairs of enantiomers. In both cases,
25 the cations are arranged in chains along the *a*-direction. A more detailed discussion of their
26 disposition along these chains will be given later on, since these are suggested to play a role in
27 the observed aggregation induced emission effect.
28
29
30
31
32
33
34
35

36 **Photophysical properties**

37
38 The qualitative molecular orbital diagram in Figure 2 summarizes the nature of the [Ir(bipy)]⁺
39 frontier molecular orbitals obtained for the cation's geometry in the Cl⁻ crystal. Due to the loss of
40 octahedral symmetry, the metal centered t_{2g}- and e_g-type orbitals, shown in red in the diagram,
41 mix significantly with themselves as well as with other ligand centered orbitals. Since the P-Ir-P
42 angle is less than 180°, we expect the interaction with the phosphine lone pairs to cause a
43 splitting of the t_{2g} orbitals by destabilizing the d_{xz} orbital with respect to the d_{xy} and d_{yz} orbitals,
44 which exhibit a small energy splitting between them.⁸⁰ As a result, the HOMO in the present
45 compounds is mainly an iridium d_{xz} orbital as shown in the diagram, while the other two t_{2g}
46
47
48
49
50
51
52
53
54
55
56
57
58
59
60

1
2
3 orbitals lie well below in energy, with several π -type orbitals of the phenyl rings of the
4 phosphines lying in between the highest occupied molecular orbital (HOMO) and the other two
5 t_{2g} -type orbitals. Due to their M-L antibonding character, the e_g -type orbitals are strongly
6 destabilized and appear rather high in energy with a significant mixture with ligand orbitals. A
7 large number of ligand centered π^* -type MOs either from the phenyl rings of the phosphines or
8 from the bipyridine appear between the t_{2g} and the e_g MOs, with the lowest unoccupied
9 molecular orbital (LUMO) being a bipyridine centered π^* -type orbital (Figure 2). The electron
10 density distribution associated with the HOMO and the LUMO are virtually identical for the
11 cation in the two crystal structures (See supplementary information, Figure S5).
12
13
14
15
16
17
18
19
20
21
22
23

24 The absorption and emission spectra at room temperature for all four [Ir(bipy)]A complexes in
25 DCM solution are shown in Figure 3. The higher energy bands in the UV-vis absorption spectra
26 for all four compounds were found between 250-300 nm and are assigned to spin-allowed
27 ligand-centered (LC) $^1\pi-\pi^*$ transitions. The lower energy bands appearing in the 350 - 425 nm
28 range are assigned to metal-to-ligand charge transfer (1MLCT and 3MLCT) transitions. As
29 expected, a similar pattern is observed for the absorbance and emission profiles of all four
30 compounds in DCM solution (Figure 3a). Emission λ_{max} values are shown in Table 1.
31
32
33
34
35
36
37
38
39
40
41
42
43
44
45
46
47
48
49
50
51
52
53
54
55
56
57
58
59
60

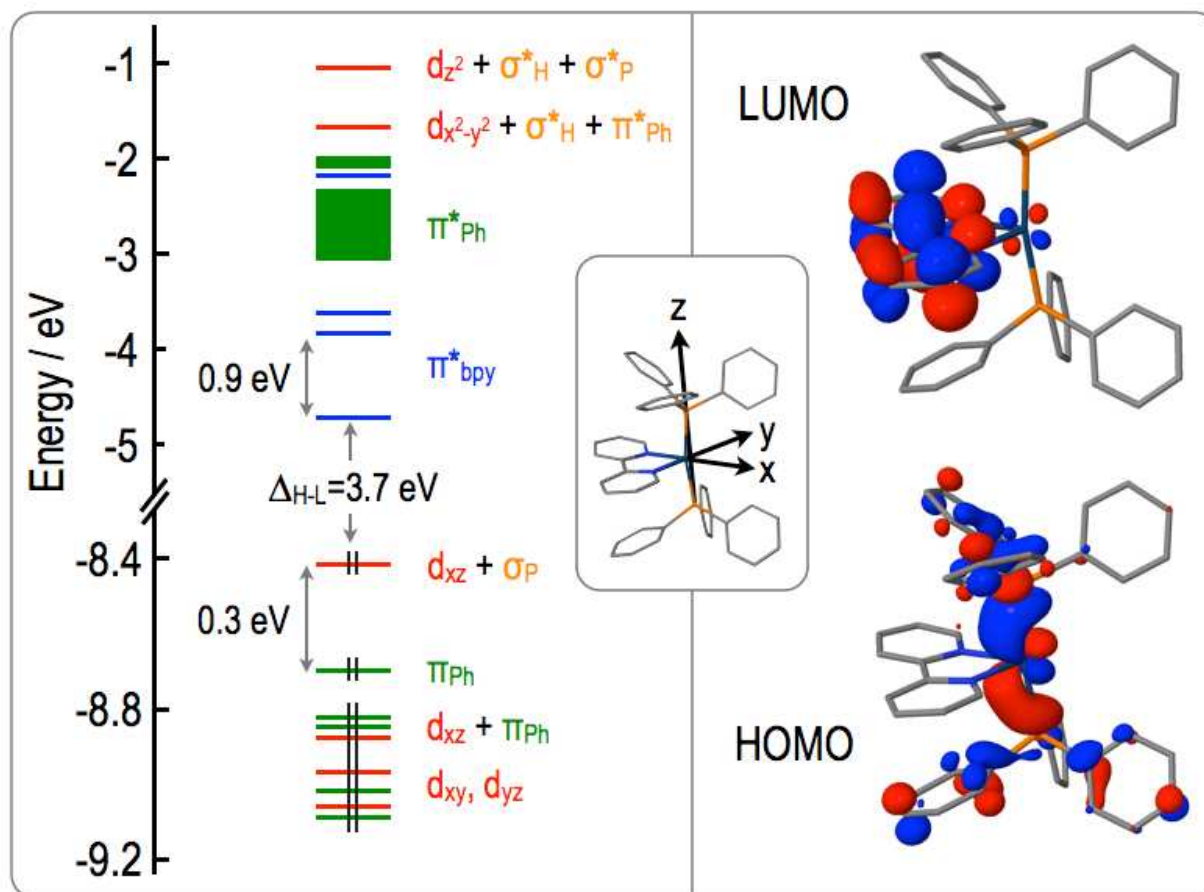


Figure 2. Molecular orbital energy diagram of **1** in the [Ir(bipy)]Cl crystal's geometry and corresponding HOMO and LUMO. Colour code: red for d-block orbitals of the iridium atom; green for π and π^* type orbitals of the phenyl rings of the phosphine ligands; blue for π^* -type orbitals of the bipyridine ligand and orange for σ -type orbitals of the phosphorous's lone pairs and the hydrogen atoms bonded directly to iridium.

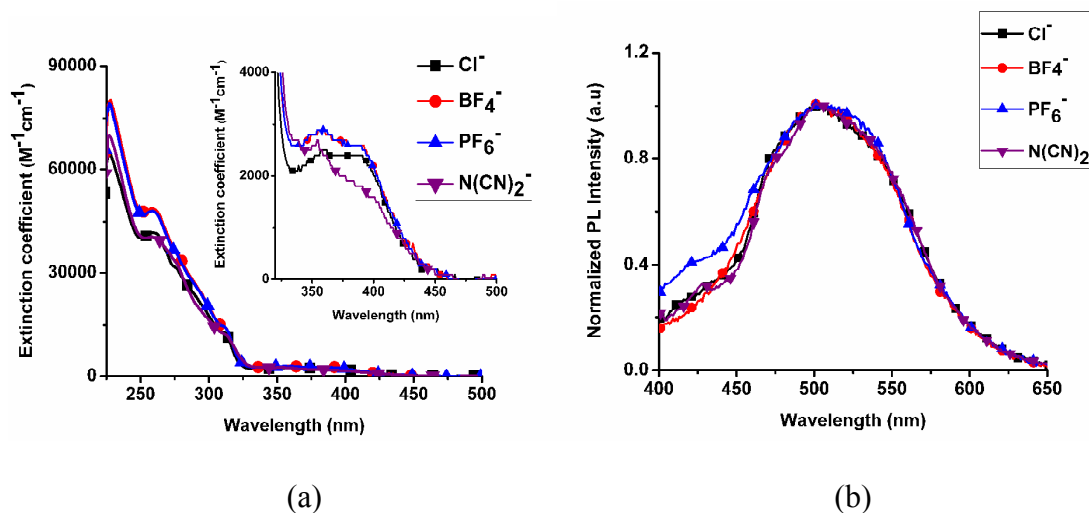


Figure 3. Absorption (a) and emission (b, λ_{exc} 385 nm) spectra for $[\text{Ir}(\text{bipy})]\text{A}$ [$\text{A}^- = \text{Cl}^-, \text{BF}_4^-, \text{PF}_6^-, \text{N}(\text{CN})_2^-$] compounds for $1 \times 10^{-5} \text{M}$ solutions in DCM.

Absorption and emission spectra of $[\text{Ir}(\text{bipy})]\text{A}$ crystals with different counterions are shown in Figure 4. While the absorption spectra are similar to those in DCM solution, the emission ones have a much more structured profile. The computed energy for the cation's LUMO is very similar in the two compounds for which we were able to solve their crystal structure, i.e. $[\text{Ir}(\text{bipy})]\text{Cl}$ and $[\text{Ir}(\text{bipy})]\text{PF}_6$, while the HOMO is 0.15 eV lower in energy in the $[\text{Ir}(\text{bipy})\text{H}_2(\text{PPh}_3)_2]\text{PF}_6$ crystal (see supplementary information, Table S3), leading to a 0.1 eV smaller HOMO-LUMO gap for the cation in crystals with PF_6^- . This is indeed the difference between the calculated excitation energies to the lowest excited triplet state of the cation, which are computed at 454 nm and 433 nm for $[\text{Ir}(\text{bipy})]\text{PF}_6$ and $[\text{Ir}(\text{bipy})]\text{Cl}$, respectively. The lowest singlet and triplet excited states have a predominant HOMO to LUMO contribution (>80%), except for the lowest triplet state of the cation in the $[\text{Ir}(\text{bipy})]\text{PF}_6$ crystal, for which the HOMO to LUMO contribution accounts just for 60% of the transition. The remaining contributions are

quite small and they basically belong to excitations to the LUMO from a d-type orbital of the iridium atom (~15%) or a π -type orbital of the bipyridine ligand (10%). Nevertheless, we can assign a strong metal to bipyridine charge transfer (MLCT) character to the S_1 and T_1 states. The vertical transition energies to the lowest excited singlet state are computed at 405 nm and 419 nm for the cation in the $[\text{Ir}(\text{bipy})]\text{Cl}$ and $[\text{Ir}(\text{bipy})]\text{PF}_6$ crystals respectively, suggesting that they are responsible of the observed band just around 400 nm in the absorption spectra.

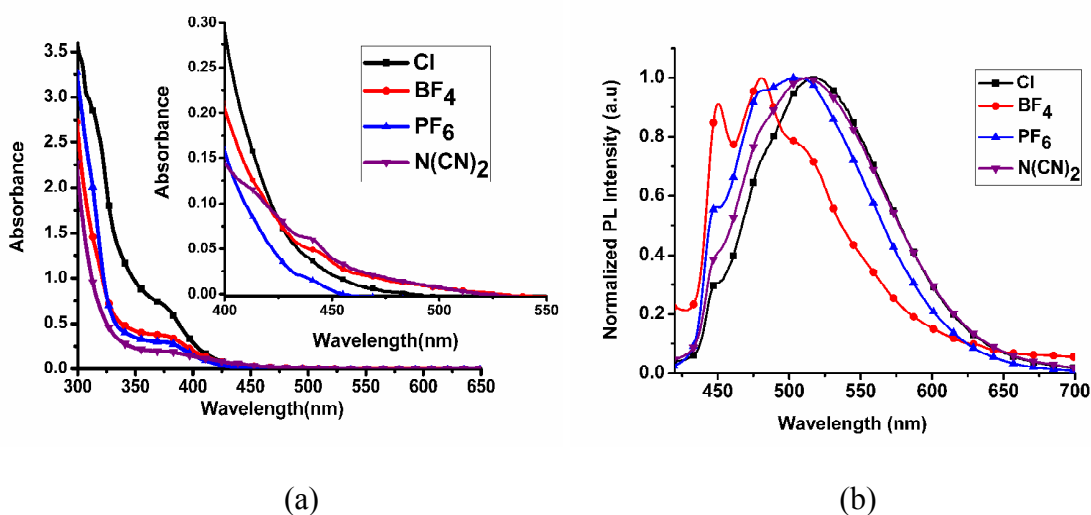


Figure 4. Absorption (a) and emission (b, λ_{exc} 385 nm) spectra in the solid state of the $[\text{Ir}(\text{bipy})]\text{A}$ crystals with $\text{A} = \text{Cl}^-$, $\text{N}(\text{CN})_2^-$, BF_4^- and PF_6^- counterions.

Table 1. Wavelengths corresponding to the maximum emission intensity along with the vibronic progressions of the crystals with different counterions in the solid state and in DCM solution. The wavelength corresponding to the maximum emission peak is indicated in boldface.

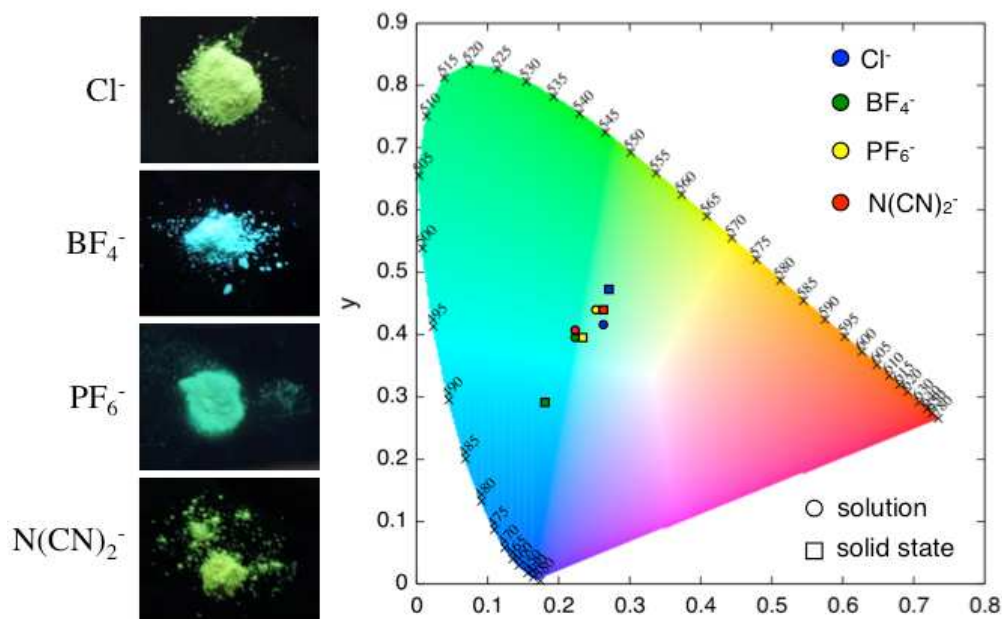
Counterion	Wavelength / nm		Quantum yield		Life time	
	Solution (DCM)	Solid State	Solution (DCM) (%)	Solid State (%)	Solution (DCM) (ns)	Aggregate State ($f_H=90\%$)
Cl^-	506	448 (sh) 512	0.018	19.85	0.95	1.6
PF_6^-	508	446 (sh) 479, 508	0.019	33.64	0.92	1.8
$\text{N}(\text{CN})_2^-$	506	446 (sh), 513	0.011	6.75	0.93	1.6
BF_4^-	505	448, 479, 514 (sh)	0.024	26.76	0.94	1.9

It is worth to stress that the computed vertical energies to the lowest triplet state (T_1) cannot be directly compared to the phosphorescence emission spectra (Figure 4), since the present calculations neither account for geometry relaxation of the triplet state, nor take into consideration vibronic coupling effects. The latter will be discussed below. Nevertheless, our calculations lead us to rule out intramolecular effects as responsible for the different phosphorescent emission properties observed for the $[\text{Ir}(\text{bipy})]\text{Cl}$ and $[\text{Ir}(\text{bipy})]\text{PF}_6$ crystals.

A notable difference in the emission spectra of the two crystals is the much better resolution of the vibrational progression structure in the $[\text{Ir}(\text{bipy})]\text{PF}_6$ case in comparison to the $[\text{Ir}(\text{bipy})]\text{Cl}$ crystal. Normal mode analysis for the cation at the minimum energy geometry for S_0 reveals that there are two breathing modes of the bipyridine ligand that may be assigned to the vibrational progression of the emission spectra. They consist of coupled asymmetric-symmetric and symmetric-symmetric breathing modes of each pyridine unit of the ligand (Figure S6), and their

1
2
3
4
5
6
7
8
9
10
11
12
13
14
15
16
17
18
19
20
21
22
23
24
25
26
27
28
29
30
31
32
33
34
35
36
37
38
39
40
41
42
43
44
45
46
47
48
49
50
51
52
53
54
55
56
57
58
59
60

computed wavenumbers are 1030 and 1038 cm^{-1} , respectively, in fairly good agreement with the gap observed in the vibrational structure of the experimental spectra (1050 cm^{-1}). In the literature⁸¹ the appearance of a resolved vibronic structure in the emission band of similar octahedral complexes has been related to a lower MLCT character and more ligand-centered π - π^* type character (LC) of the excited state. As discussed above, our computational study does not suggest that the nature of the emitting triplet state should differ significantly in the two crystals, so that we expect a similar MLCT character for emission in the two cases and for this reason we suggest that the differences observed in the vibronic structure of the cation in the two studied crystals are caused by different intermolecular interactions. A difference in the colour of the emitted light was observed for the four compounds under excitation at 365 nm, as shown in Figure 5. The values of the xy chromaticity coordinates (Table S4) and further details regarding their calculation may be found as Supplementary Information.



1
2
3 **Figure 5.** *Left.* Pictures of the emitting [Ir(bipy)]A crystals with different counter ions: Cl⁻, BF₄⁻,
4
5 PF₆⁻ and N(CN)₂⁻. *Right.* Chromaticity diagram (standard CIE (2°) 1931 colour space⁸²) for the
6
7 synthesized complexes in DCM and solid state.
8
9

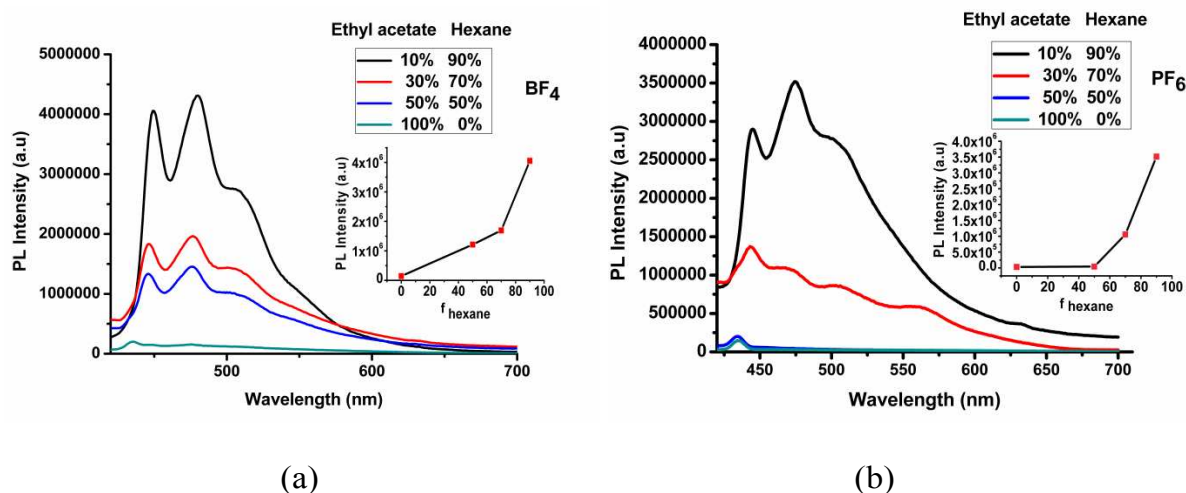
10
11
12 Amongst the four different crystals, the one with BF₄⁻ shows a more bluish colour than the rest,
13
14 which follow a trend in their emission colours, going from greenish to more yellow as we move
15
16 from PF₆⁻ to N(CN)₂⁻ and Cl⁻. On the other hand, as expected, the colour of the weak emission of
17
18 all the complexes in DCM is very similar, showing that the differences arise from intermolecular
19
20 interactions upon aggregation.
21
22
23

24 25 **Aggregation Induced Emission** 26

27
28 All four investigated compounds present quite weak emission intensities when dissolved
29
30 in common organic solvents, such as DCM, trichloromethane or tetrahydrofuran, while in
31
32 the solid state their phosphorescence emission becomes much more intense. To
33
34 investigate and characterize the observed AIE effect, the four complexes were dissolved
35
36 in ethyl acetate and then a gradually increasing amount of hexane was added (hexane
37
38 fraction (f_H) 0-90%, concentration = 1×10^{-4} molL⁻¹). Since the complexes are not soluble in
39
40 hexane, the extent of aggregation should increase with higher hexane fractions. As shown
41
42 in Figure 6 and 7, the PL intensity of [Ir(bipy)]BF₄ increases steadily with the fraction of
43
44 hexane ($f_H = 0-70\%$) in the mixture, while a sharp enhancement of the PL intensity was
45
46 observed when increasing the hexane fraction from 70% to 90%. The PL intensity at $f_H =$
47
48 90% was found to be about 25.6 times higher than for the solution in pure ethyl acetate.
49
50 Similarly, the PL intensity of compounds [Ir(bipy)]PF₆ and [Ir(bipy)]Cl increased at $f_H =$
51
52 90% to 27.9 and 116 times that in ethyl acetate solutions, respectively. In case of
53
54
55
56
57
58
59
60

[Ir(bipy)]N(CN)₂, the PL intensity increased slowly to $f_H = 70\%$, but at $f_H = 90\%$ a decrease of the intensity was observed. The PL intensity of [Ir(bipy)]N(CN)₂, at $f_H = 70\%$ and $f_H = 90\%$ is about 7.8 and 6.9 times larger, respectively as compared to the intensity for the parent solution in pure ethyl acetate.

To further investigate the decrease of the PL intensity of complex [Ir(bipy)]N(CN)₂ for $f_H = 70\%$, we took transmission electron microscopy (TEM) images with electron diffraction (ED) for samples of this complex. The TEM image clearly showed the existence of nanowire-like aggregates (90-230 nm range) at $f_H = 90\%$. The absence of a clear bright ring in electron diffraction supported the formation of amorphous molecular aggregates (Figure 8). The absolute quantum yields for [Ir(bipy)]A (A = Cl, PF₆, BF₄ and N(CN)₂) were estimated in powder form and found to be 19.85% (Cl), 33.64% (PF₆), 26.76% (BF₄) and 6.75% (N(CN)₂), respectively, while the relative quantum efficiencies in solution (in DCM, with respect to coumarin 153 dissolved in degassed ethanol, QE = 0.38) were observed to be very low, *i.e.*, 0.018% (Cl), 0.019% (PF₆), 0.024% (BF₄), and 0.011% (N(CN)₂). These facts support that all four compounds have an enhanced emission in the solid state.



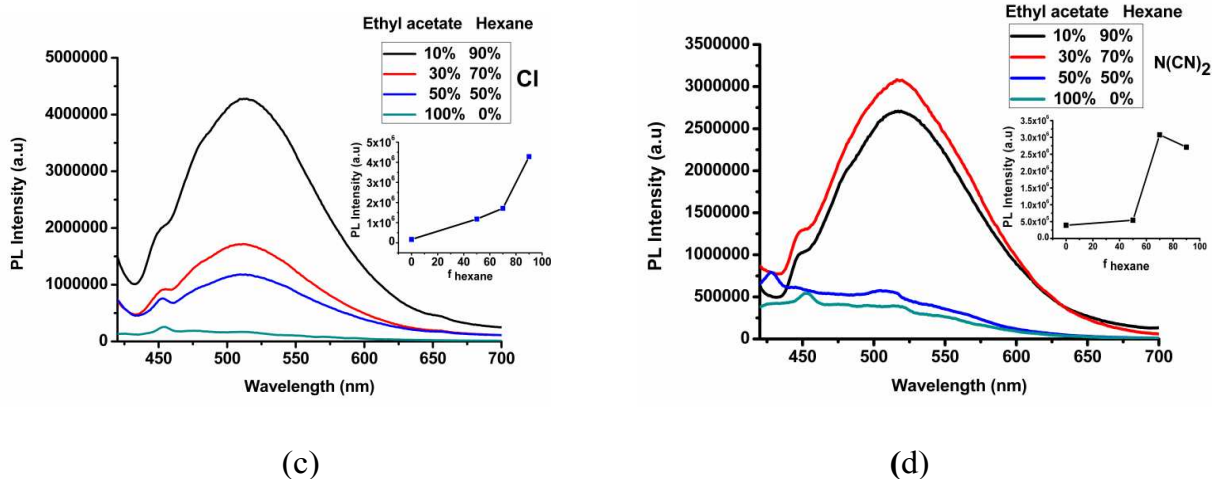


Figure 6. PL spectra for the $[\text{Ir}(\text{bipy})]\text{A}$ compounds in ethyl acetate/hexane mixtures with λ_{exc} at 385 nm. (a) BF_4 , (b) PF_6 , (c) Cl (d) $\text{N}(\text{CN})_2$ insets: evolution of the PL intensity of complexes at different f_H (0-90 %) fractions.

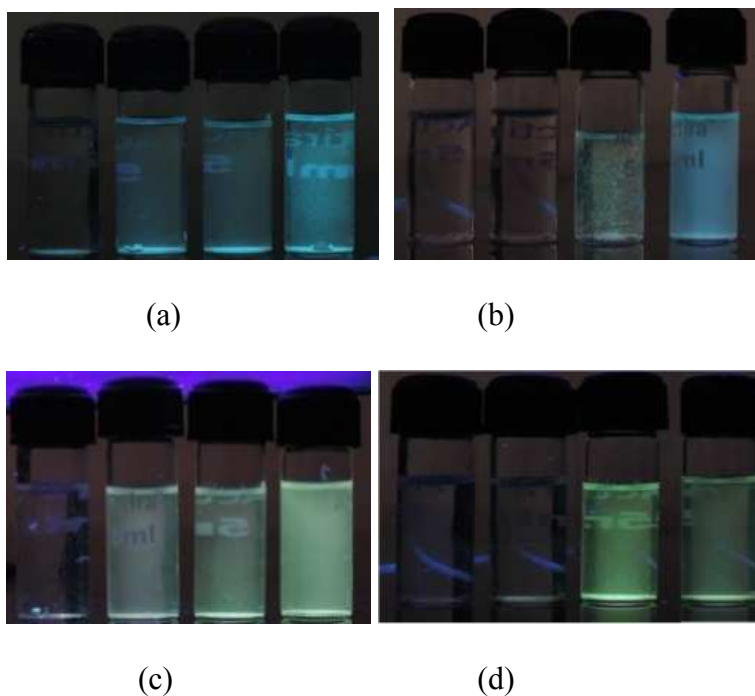
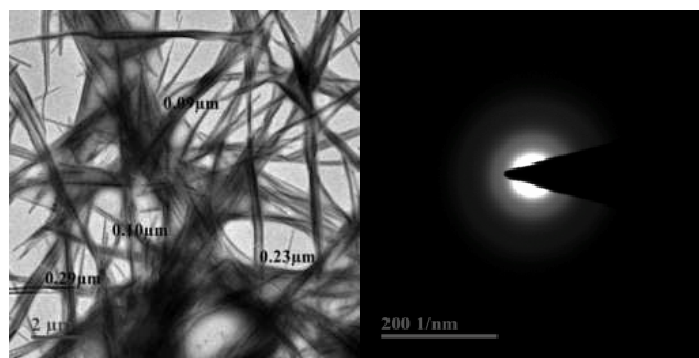


Figure 7. Luminescent images of $[\text{Ir}(\text{bipy})]\text{A}$ in ethyl acetate-hexane at different fractions of hexane (0% 50% 70% and 90% , left to right) keeping the $1 \times 10^{-4} \text{M}$ concentration of the solution.



(a)

(b)

Figure 8. (a) TEM image of nanoaggregates of $[\text{Ir}(\text{bipy})]\text{A}$ ($\text{A} = \text{N}(\text{CN})_2$) formed in ethyl acetate-hexane mixtures with 90% hexane fraction. (b) Electron diffraction (ED) pattern of the nanoaggregates showing amorphous nature of the aggregate

Let us consider four possible sources for emission enhancement upon aggregation of the coordination complexes studied in this work:

- (i) Packing forces in the aggregated state induce a **reorganization of the coordination sphere of the metal atom** large enough to change the nature of the emitting state. In this scenario, the change of the coordination sphere should enhance spin-orbit coupling in the emitting state as compared to that in diluted solutions with a result of an increase in the efficiency of the radiative deactivation pathway.
- (ii) The aggregation process leads to **strong intermolecular delocalization of the ground state, the emitting state, or both**. This change will affect mainly the efficiency of the radiative pathway, although it is not easy to predict a priori if the emission intensity should increase or decrease since it will depend largely on the degree of delocalization of the emitting and the ground states and this degree of localization is difficult to describe from a computational point of view.

- 1
2
3 (iii) Packing forces in the aggregate state **restrict the internal motion (RIM)** in the cations,
4 most importantly internal rotations and low frequency, large amplitude vibrations in the
5 emitting molecule. The non-radiative deactivation process is well described by a first
6 order rate equation whose constant depends on two parameters: the strength of the
7 coupling between the initial (emitting) state and the final (ground state) as well as the
8 density of vibronic states of the ground state at the energy of the emitting state.⁸³⁻⁸⁶
9
10 Considering that the presence of nearby molecules should not induce great changes in the
11 coupling between the initial triplet and the final singlet state, the leading ingredient
12 should be a decrease of the ground state's density of vibrational states. Steric congestion
13 and interlocking of mobile parts would hinder large amplitude movements upon
14 aggregation with an increase in their vibrational frequencies and the associated decrease
15 in the density of states leading to a smaller rate constant for the non-radiative process.
16
17 (iv) Another possibility is that packing forces in the crystal could impose **restrictions along**
18 **the molecular geometry relaxation on the emitting state potential energy surface.**
19 Thus, the emitting state in the solid would be less distorted than in solution, leading to a
20 decrease of the Franck-Condon factors, which would result in a decrease of the non-
21 radiative decay rate constant
22
23
24
25
26
27
28
29
30
31
32
33
34
35
36
37
38
39
40
41
42
43
44
45

46 Of course more than one of these mechanisms may occur simultaneously in a same crystal, and
47 discerning if there is a clear effect causing the enhancement of emission upon aggregation is
48 extremely difficult. The present case, where we have the same emitting cation in different
49 crystalline environments, offers an excellent opportunity to try to shed some light on these
50 questions, although we will unfortunately have to limit our study to the comparison between
51
52
53
54
55
56
57
58
59
60

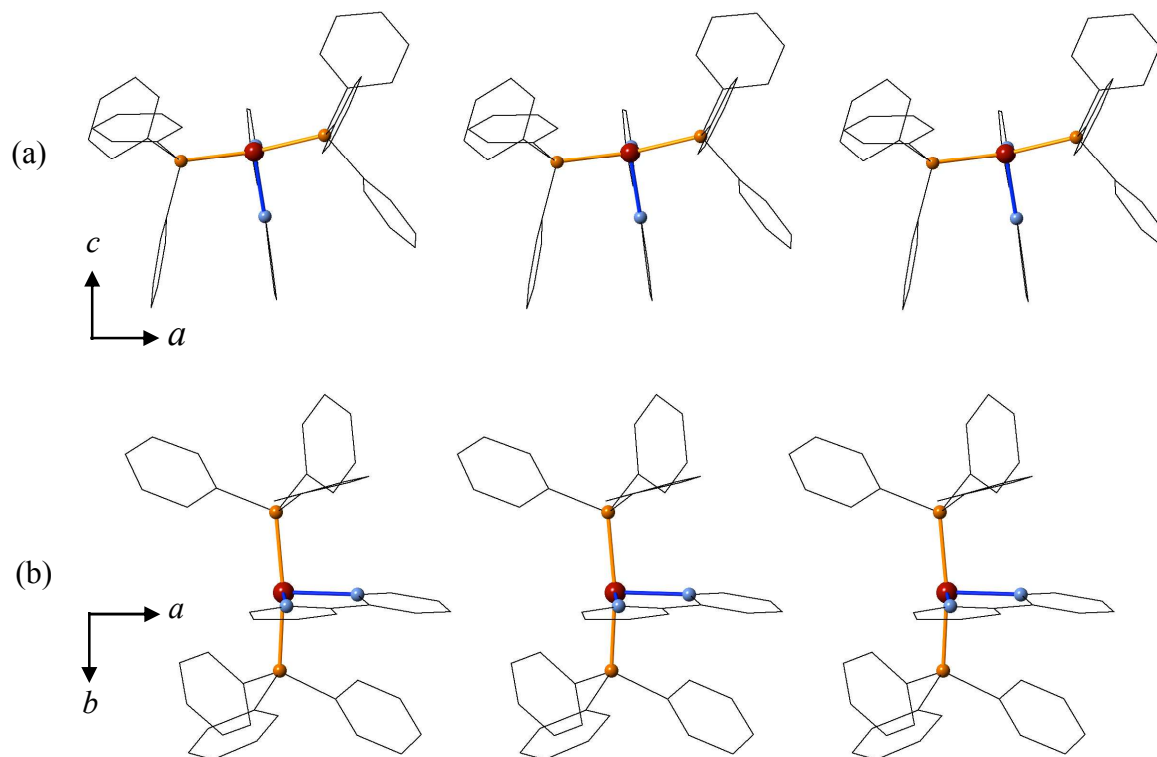
1
2
3 crystals with the Cl^- and PF_6^- counterions, for which we have been able to obtain X-ray resolved
4
5 crystalline structures that will be considered to offer a proper model for the types of interactions
6
7 that may be present in amorphous aggregates.
8
9

10
11
12 Since the principal features of the common $[\text{Ir}(\text{bipy})]^+$ cation at the molecular level, both
13
14 regarding its atomic and electronic structure have already been discussed, and intramolecular
15
16 effects don't seem to be responsible for the enhanced emission in aggregate state, herein we will
17
18 focus on the role of the crystal structure. In particular, we will discuss the different molecular
19
20 packing modes and their possible implications in the electronic structure of the crystals such as
21
22 electronic delocalization and π -stacking.
23
24
25
26
27
28

29 **Intra-chain interactions**

30
31 The $[\text{Ir}(\text{bipy})]^+$ cations are packed into chains along the a -direction of the crystals (Figure
32
33 9). The fundamental difference between the packing modes in the $[\text{Ir}(\text{bipy})]\text{Cl}$ and
34
35 $[\text{Ir}(\text{bipy})]\text{PF}_6$ crystals is the way in which the molecules dispose with respect to the chain
36
37 direction. In the $[\text{Ir}(\text{bipy})]\text{PF}_6$ crystal, the molecular P-Ir-P axis is oriented along the chain
38
39 axis (Figure 9a), while it lies approximately perpendicular to it in the $[\text{Ir}(\text{bipy})]\text{Cl}$ crystal
40
41 (Figure 9b). This difference in the orientation of the molecule with respect to the chain
42
43 axis in the two cases may be important for the RIM mechanism, since in the $[\text{Ir}(\text{bipy})]\text{PF}_6$
44
45 crystal, for which a relatively stronger AIE effect is observed, interlocking between the
46
47 highly movable phenyl rings of neighbouring molecules may effectively restrict their
48
49 motion, while in the $[\text{Ir}(\text{bipy})]\text{Cl}$ crystal, the interaction between neighbours is mainly
50
51
52
53
54
55
56
57
58
59
60

1
2
3 between the rigid bipyridine and mobile triphenylphosphine fragments, which may result
4
5 in a less effective RIM.
6
7



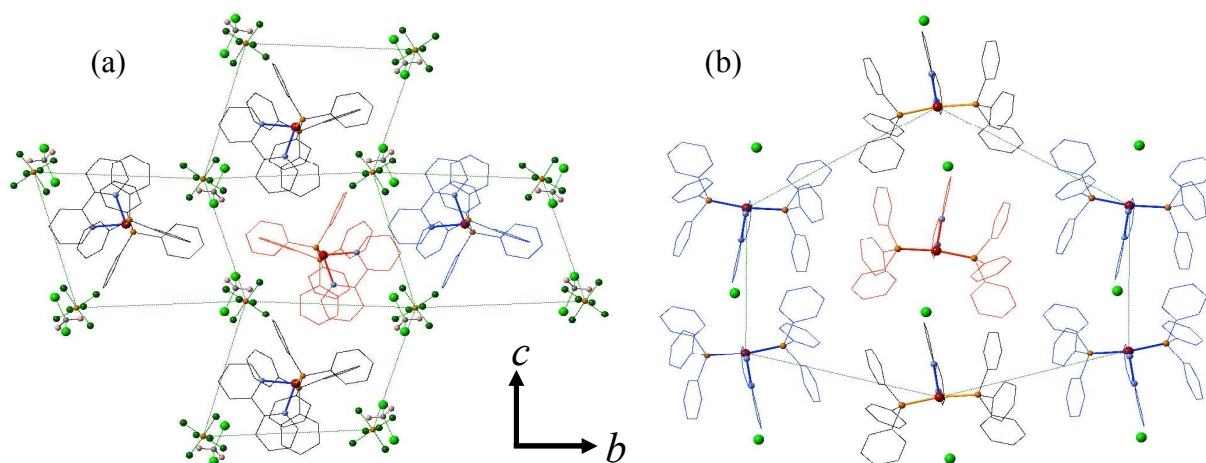
37 **Figure 9.** Chains in the (a) $[\text{Ir}(\text{bipy})]\text{PF}_6$ and (b) $[\text{Ir}(\text{bipy})]\text{Cl}$ crystal structures. Colour code: Ir-P
38 bonds (orange) and Ir-N bonds (blue). Hydrogen atoms are not shown for the sake of clarity.
39
40
41
42
43

44 **Inter-chain interactions**

45
46 In the $[\text{Ir}(\text{bipy})]\text{PF}_6$ crystal structure, shown in Figure 10a in a view along the direction of
47 the chains, and taking the chain with the ligands coloured in red as our reference, there
48 are four chains of alternating PF_6^- counterions and DCM molecules forming a more or less
49 square prism around the reference chain. There are also four additional cation chains that
50 interact with the reference chain through the faces of this square prism. The neighbouring
51
52
53
54
55
56
57
58
59
60

1
2
3 chains at the left and right side of the central one in the figure are shifted along the chain
4 direction with respect to the central chain so that the iridium atoms do not have the same
5 coordinate along the axis parallel to the chain direction, in contrast to the neighbouring
6 chains shown above and below the central one in the figure, which lie on the same plane
7 as the reference cation's chain.

15 In the $[\text{Ir}(\text{bipy})]\text{Cl}$ crystal, where anions are much smaller, each chain is surrounded by six
16 neighboring cationic chains (Figure 10b) in an arrangement reminiscent of a compact hexagonal
17 packing for perfect cylinders. In this case, the four neighboring chains shown to the left and the
18 right of the central one are also shifted along the chain direction with respect to the central chain,
19 while all the iridium atoms from chains represented above and below lie in the same plane
20 perpendicular to the a -direction (yz -plane of Figure 10b). As it can be appreciated in the figure,
21 since in this case the P-Ir-P axis is approximately perpendicular to the axis of the chains,
22 molecules from different chains face each other mainly through the triphenylphosphine ligands.
23 The Cl^- counterions occupy in this case the voids in the structure left between the rigid bipyridine
24 ligands of one molecule and the hydride ligands on the neighboring one.



1
2
3 **Figure 10.** Interactions between chains that align along the *a*-direction in the (a) [Ir(bipy)]PF₆
4 and (b) [Ir(bipy)]Cl crystal structures.
5
6
7
8
9

10 In both crystals, there are relevant interactions between some hydrogen atoms on the bipyridine
11 ligand or the phenyl rings and the counterions. In the [Ir(bipy)]Cl crystal, there are short
12 C–H···Cl contacts that range from 2.7 to 3.0 Å (Figure S7 and S8), while in the [Ir(bipy)]PF₆
13 crystal, there are C–H···F interactions that lie in the range of 2.4 to 3.1 Å (Figure S9 and 10).
14
15
16
17
18

19 More important for our purposes, there are also significant inter-chain interactions in the two
20 cases. In the [Ir(bipy)]PF₆ crystal, C–H··· π interactions^{87, 88} are found between the cation chains
21 highlighted in blue and red in Figure 10a. These interactions between the rigid bipyridine
22 fragment and the mobile phenyl rings (Figure 11) may indeed play an important role in the
23 restriction of the motion of these rotors. No other relevant interactions between the rigid
24 fragments of the cations and their phenyl rings were found for the remaining chains of the
25 [Ir(bipy)]PF₆ crystal. In contrast, for the [Ir(bipy)]Cl crystal, the C–H··· π distances are much
26 larger, excluding the possibility of this type of interactions to be relevant in this case. The
27 principal interactions between the neighboring chains and the reference one highlighted in red in
28 the [Ir(bipy)]Cl crystal (Figure 10b) are with the triphenylphosphine ligands on the chains
29 highlighted in blue, in which interlocking of the phenyl rings would restrict motions in the solid
30 state.
31
32
33
34
35
36
37
38
39
40
41
42
43
44
45
46
47
48
49
50
51
52
53
54
55
56
57
58
59
60

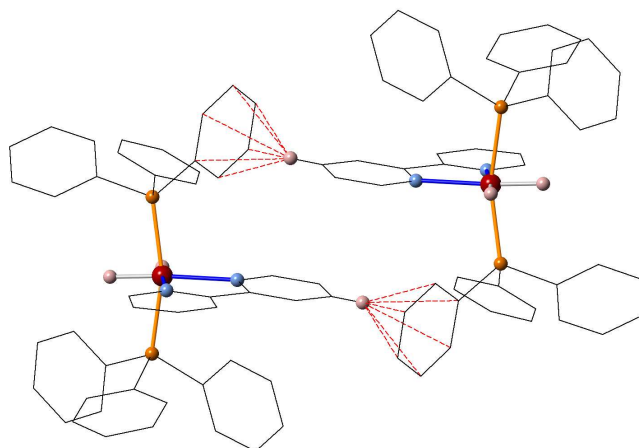
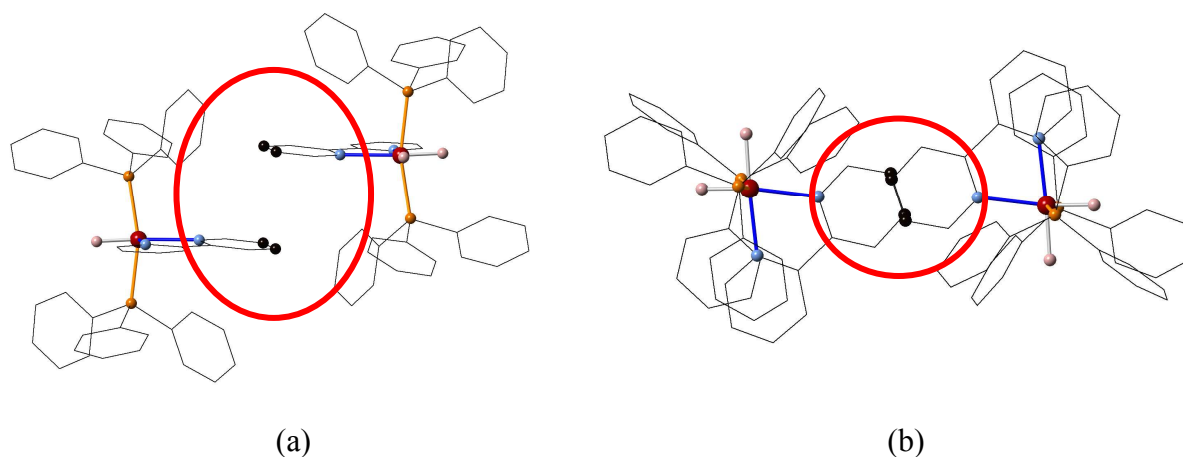


Figure 11. Inter-chain C-H $\cdots\pi$ in the [Ir(bipy)]PF₆ crystal structure.

The only interactions between chains that may have significant electronic implications in their photophysical properties, that is electronic delocalization and/or π -stacking interactions, are those between the chains highlighted in red and blue in the [Ir(bipy)]PF₆ crystal (Figure 10a), where the π -systems of their bipyridine ligands are susceptible to have a non negligible overlap (Figure 12). The shortest C-C distance between the two coplanar bipyridine ligands is approximately 3.47 Å. Although the distance between the two ligands is short enough to be below the upper limit of what may be considered as a π -stacking interaction,^{89, 90} the vertical overlap between them is very poor, since the two ligands are quite displaced with respect of a complete alignment, limiting the overlap of π -type orbitals to just two carbon atoms on each bipyridine fragment. In light of this qualitative analysis, we can exclude significant electronic cooperative effects between neighboring complexes as the source of the different emission properties in the [Ir(bipy)]Cl and [Ir(bipy)]PF₆ crystals.

Summarizing the previous discussion, we arrive at the following conclusions: the involvement of the phenyl rings of the flexible triphenylphosphine ligand in intermolecular interactions is clearly

1
2
3 recognizable in the two crystal structures. Namely, as interlocking interactions between
4 neighboring molecules in each chain in the $[\text{Ir}(\text{bipy})]\text{PF}_6$ crystal with additional attractive
5 $\text{C}-\text{H}\cdots\pi$ interactions between chains and interlocking of the phenyl rings of neighboring
6 molecules on different chains in the $[\text{Ir}(\text{bipy})]\text{Cl}$ crystal. Since all other sources of possible AIE
7 can be discarded from the comparative analysis of the crystal structures, it seems plausible to
8 assume that the establishment of these intermolecular interactions will significantly hinder the
9 molecular motion of the phenyl rotors in the aggregated state.
10
11
12
13
14
15
16
17
18
19



38 **Figure 12.** Side view (a) and top view (b) of a possible π -stacking interaction between two
39 cations in the $[\text{Ir}(\text{bipy})]\text{PF}_6$ crystal.
40
41
42
43
44
45
46
47
48
49

50 **Molecular relaxation of the emitting state**

51
52 The optimized geometry of the lowest excited triplet state of **1** has important differences with
53 respect to the ground state optimized geometry and the molecular structure in the crystal. In fact,
54 our calculations point towards a decrease of the P-Ir-P angle of approximately 20° upon
55
56
57
58
59
60

excitation to the T_1 state (Table 2) due to the participation of the phosphorous's lone pair in the t_{2g} -type orbitals of the cation. This considerable geometry change in the MLCT triplet state may in fact have an important contribution to the factors responsible for the enhanced phosphorescence in the solid state since the triplet state in the aggregate may not be able to fully relax, as opposed to in solution. As a result we might expect smaller Franck-Condon factors and a decrease of the non-radiative decay rate constant in the crystal with respect to in solution,⁴⁸ enhancing phosphorescence in the solid state.

Table 2 P-Ir-P angles for different structures of **1**.

structure	Cl ⁻ crystal	PF ₆ ⁻ crystal	S ₀	T ₁
P-Ir-P angle (°)	168	162	164	140

Crystallization Induced Emission (CIE):

In a further investigation of the luminescent properties of the [Ir(bipy)]A compounds, [Ir(bipy)]Cl was found to exhibit an unusual crystallization induced emission behavior.

With exposure of the green emitting solid complex, [Ir(bipy)]Cl ($\lambda_{\max} = 519$ nm) to DCM or chloroform, it transformed into a faint yellow emitting complex ($\lambda_{\max} = 548$ nm). Meanwhile, the yellow emissive form (Y) was reverted back to green emissive form (G) after grinding followed by fuming with acetone /or ethyl acetate /or benzene.

In another experiment, the Y form was coated on a filter paper and the word "BITS" was written on it with the help of a capillary tube with acetone (Figure 13). Interestingly, the observed transformation of Y into G only in the zone where the word 'BITS' was written hints to the

1
2
3 potentiality of this compound for applications in the fields of optical recording and pressure-
4
5 sensing. This drastic change in the emission behavior may be attributed to the solvent/vapor
6
7 induced recrystallization upon exposure to acetone, which can be observed in Figure S11, where
8
9 a drop of acetone produced a drastic change in the emission behavior of [Ir(bipy)]Cl. The
10
11 presence of DCM in the Y form was revealed by thermogravimetric analysis (TGA), which
12
13 showed a weight loss in the range of 50⁰C-150⁰C compatible with the loss of one molecule of
14
15 DCM (Figure S12).
16
17

18
19 From these experiences, it may be deduced that the G form was converted into the Y form upon
20
21 exposure to DCM or chloroform vapors. In this sense, these two solvents seem to be
22
23 responsible of the formation of amorphous aggregates in the Y form by intermolecular
24
25 interactions with the complex.
26
27
28
29
30
31



32
33
34
35
36
37
38
39
40
41
42 **Figure 13.** A filter paper coated by complex [Ir(bipy)]Cl where the word 'BITS' was written by
43
44 using a capillary tube loaded with acetone.
45
46
47
48

49 To further investigate this hypothesis, powder X-ray diffraction (PXRD) measurements for the
50
51 two different samples were performed (Figure 14). The PXRD of the G form showed sharp and
52
53 intense peaks, which were in good agreement with the simulated PXRD, indicating that G
54
55 corresponds to a well-ordered and crystalline material. For the Y form, the appearance of less
56
57
58
59
60

intense and broader peaks suggests an amorphous nature for the aggregate. It is needless to say that the position of the peaks (2θ) of the G and Y forms remains the same.

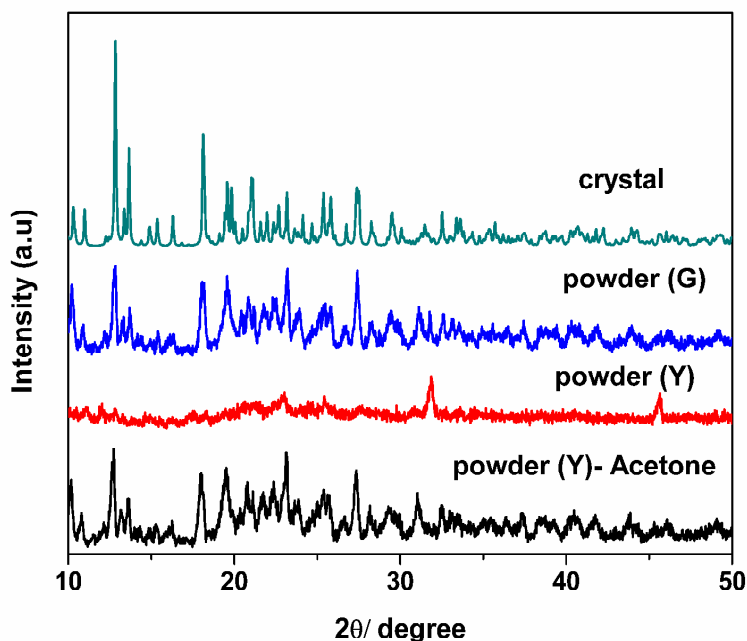


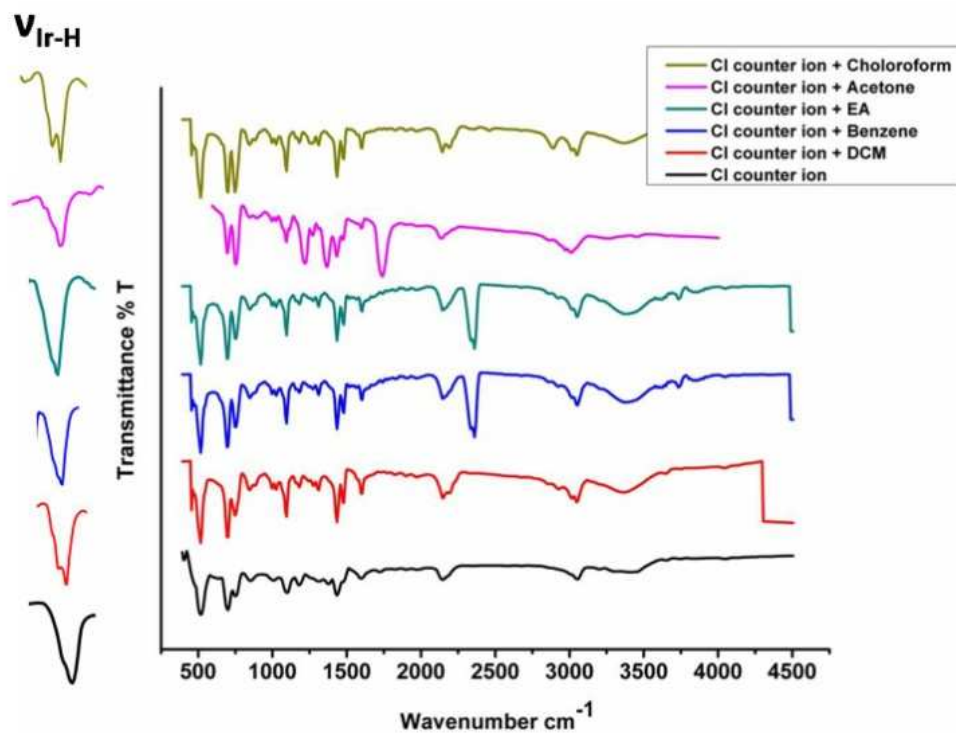
Figure 14. Power X-ray diffraction pattern of [Ir(bipy)]Cl recorded for various states (a) collected from crystal data (b) from the green powder G (c) the yellow powder Y and (d) grinding the Y powder lightly followed by exposure to acetone.

Thus, the CIE behavior of [Ir(bipy)]Cl can be ascribed to changes in the amorphous/crystalline nature obtained by fuming (DCM/chloroform) and grinding followed by fuming (acetone, ethyl acetate or benzene).

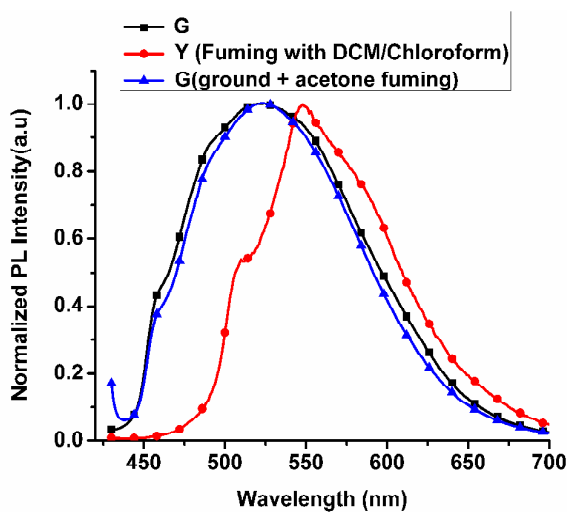
In a further investigation, the differential scanning calorimetry (DSC) thermograms of the Y form showed exothermic peaks (recrystallization temperatures) at ~ 90 °C while the melting temperature was found to be ~ 240 °C (Figure S13). These results indicate that the yellow emitting complex is in a meta-stable amorphous aggregation state that undergoes crystallization upon heating. The green emitting samples obtained after grinding followed by fuming do not

1
2
3 show any recrystallization peak in DSC (Figure S13), suggesting that the amorphous yellow
4 emitting samples revert back to the original G form. These observations are useful to shed some
5 light on the observed CIE behavior for the chloro-complex, showing that the changes in the
6 emission colour are due to modifications in the molecular packing upon grinding/fuming.
7

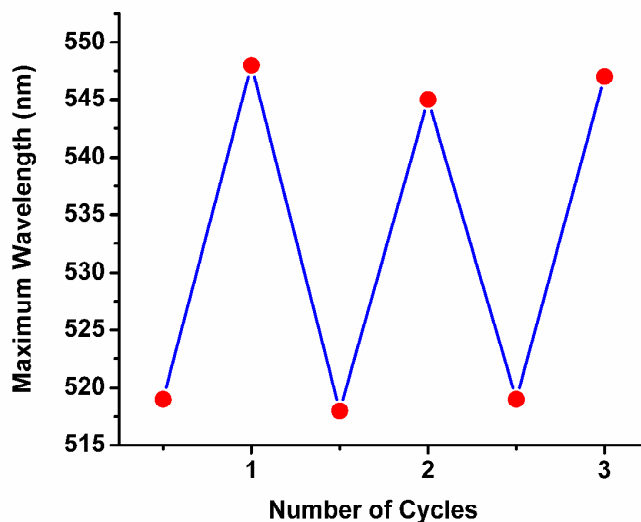
8
9
10 To further complement the information on these issues, the IR spectrum was recorded to
11 investigate possible interactions between different solvent molecules with Ir(bipy)]Cl (Figure
12 15). The IR spectra for the green emitting complex showed a broad signal at 2142 cm^{-1} ,
13 attributed to the Ir-H stretching frequency, that is split into two peaks (2145 and 2186 cm^{-1}). This
14 splitting of the Ir-H stretching frequency can be attributed to the interaction of DCM molecule
15 with the hydride ligand of the complex. This result encouraged us to try to study the interaction
16 of the cation with other solvents by analyzing the spectral features of this peak. The Ir-H
17 stretching mode was found to give rise to a broad peak at 2143 cm^{-1} , 2145 cm^{-1} and 2142 cm^{-1} in
18 presence of benzene, ethyl acetate, and acetone, respectively, while in presence of chloroform,
19 two split peaks (2143 and 2192 cm^{-1}) were observed (Figure 15). Taking these observations into
20 account, the changes in the hydride peak in the FTIR spectra for the Y and G forms of
21 Ir(bipy)]Cl leads us to propose the involvement of an interaction between the hydride of the
22 complex and the chloro-containing solvents (DCM/chloroform). After applying external stimuli
23 (grinding followed by fuming), these weak hydrogen-bond interactions might be broken with the
24 resulting change of the emission colour from yellow to green. These interactions can be rebuilt
25 after recrystallizing the complex in DCM (Figure 16),⁹¹ allowing the process to be reversed.
26
27
28
29
30
31
32
33
34
35
36
37
38
39
40
41
42
43
44
45
46
47
48
49
50
51
52
53
54
55
56
57
58
59
60



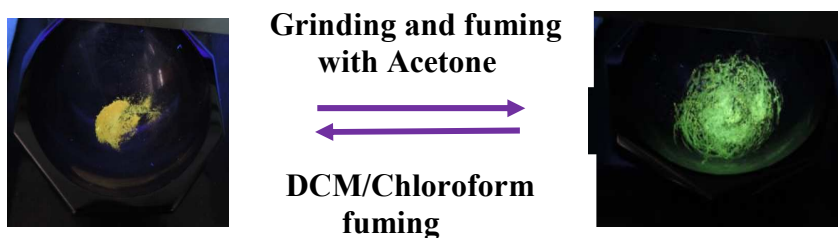
32 **Figure 15.** IR spectrum of the complex was recorded after exposure of different solvents;
33 showing the interaction of solvents with [Ir(bipy)]Cl.
34
35
36
37
38
39
40
41
42
43
44
45
46
47
48
49
50
51
52
53
54
55
56
57
58
59
60



(a)



(b)



(c)

Figure 16. (a) Solid state emission spectra of $[\text{Ir}(\text{bipy})]\text{Cl}$, representing the change in the emission maxima after exposure to DCM/chloroform and after grinding followed by fuming (acetone); (b) Reversibility response of $[\text{Ir}(\text{bipy})]\text{Cl}$ after sequential exposure to DCM/chloroform and grinding followed by fuming (acetone); (c) colour change after CIE effect.

CONCLUSIONS

Crystals based on the $[\text{Ir}(\text{bipy})\text{H}_2(\text{PPh}_3)_2]^+$ cation with the Cl^- , $\text{N}(\text{CN})_2^-$, BF_4^- and PF_6^- counteranions were synthesized, all of them exhibiting an enhancement of the phosphorescence emission upon aggregation. Crystal structures could only be determined for the Cl^- and PF_6^-

1
2
3 crystals and the corresponding iridium(III) cations have been studied in detail with the aid of
4
5 quantum chemical calculations and their emission properties discussed from a qualitative point
6
7 of view by analyzing the crystal packing, the frontier molecular orbitals and the calculation of
8
9 the nature of the low-lying excited states.

10
11 Our analysis shows that the lowest triplet state of the $[\text{Ir}(\text{bipy})\text{H}_2(\text{PPh}_3)_2]^+$ cation originates from
12
13 a HOMO to LUMO transition with a strong MLCT character that is not greatly affected by the
14
15 relative minor differences in the coordination geometry induced by the crystalline environment.
16
17

18
19 The arrangement of the cations in the two crystals allow interlocking interactions between the
20
21 triphenylphosphine ligands on neighboring molecules that are suggested to lead to a significant
22
23 restriction of the motion of the phenyl rotors in aggregates. In addition, C-H $\cdots\pi$ interactions
24
25 between the bipyridine and the triphenylphosphine ligands are present in the PF_6^- crystals
26
27 leading to further hindering of these internal motions. The existence of relevant intermolecular π -
28
29 stacking interactions has been ruled out by analyzing the crystal packing.
30
31

32
33 Since the changes in coordination geometry and electronic delocalization seem to be out of
34
35 question, the most plausible origin of the AIE effect in the studied compounds appears to be the
36
37 restriction of internal motion (RIM mechanism). The presence of six phenyl rings that can
38
39 experience large amplitude internal rotations around the P-C axis should lead to a relatively high
40
41 density of states of vibrational modes in solution that would decrease dramatically upon
42
43 aggregation and restriction of their movement. The larger phosphorescence quantum yield
44
45 observed for the crystals with PF_6^- seems to hint at a larger RIM in this case, perhaps due to the
46
47 additional C-H $\cdots\pi$ interactions found in the crystal. The observation of some vibrational
48
49 structure in the spectra for the PF_6^- case seems also to hint to a stronger restriction of the low
50
51 frequency modes that would result in a larger spacing of their associated vibrational states and a
52
53
54
55
56
57
58
59
60

1
2
3 more structured spectrum in which the vibrational progressions of the modes affected by the
4
5 electron transfer are not blurred by the quasi continuum of low frequency modes active in
6
7 solution or in loosely packed crystals. Interestingly, it was found that the chloro-complex showed
8
9 CIE and the exploration of the mechanism for this phenomenon using IR spectroscopy reveals
10
11 that the formation/destruction of non-covalent interactions between chlorinated solvents and the
12
13 hydride ligand of the complex seem to be involved in the observed reversible colour changes.
14
15
16
17
18
19

20 ASSOCIATED CONTENT

21
22 Text, figures, tables, ¹H NMR, and HRMS spectra, X-ray structure analyses including tables of
23
24 bond and lengths and angles. The supporting information is available free of charge on the ACS
25
26 Publication website at <http://pubs.acs.org>. All crystallographic data have been deposited with the
27
28 Cambridge Crystallographic with CCDC reference numbers 1435821-1435822. These data can
29
30 be obtained free of charge via www.ccdc.cam.ac.uk/conts/retrieving.html (or from the CCDC, 12
31
32 Union Road, Cambridge CB2 1EZ, UK; fax: + 44 1223 336033; e-mail:
33
34 deposit@ccdc.cam.ac.uk).
35
36
37
38
39
40
41
42

43 AUTHOR INFORMATION

44
45 Corresponding Authors

46
47
48 * Email for I.R.L.: ir_laskar@pilani.bits-pilani.ac.in
49
50
51
52

53 Notes

54
55 The authors declare no competing financial interest
56
57
58
59
60

1
2
3 Author Contributions
4
5

6 ‡These two authors contributed equally to the development of this manuscript.
7
8

9
10 **ACKNOWLEDGMENT**
11

12 We thank gratefully ‘Department of Science and Technology (DST), Govt. of India’ (project
13 No.: SB/S1/IC-13/2014) and the Spanish *Ministerio de Economía y Competitividad* (project
14 CTQ2015-64579-C3-3-P) for financial support. The ‘UGC-SAP’ and ‘DST-FIST’ programs for
15 the chemistry department, BITS Pilani have been acknowledged for instrumental supports. We,
16
17 also thank IISER Mohali for the use of their single crystal X-ray diffraction and NMR research
18 facilities. D.C. thanks the Basque Government (project IT588-13) and IKERBASQUE, Basque
19 Foundation for Science for financial support. C.C. is indebted to the Spanish ‘Ministerio de
20 Economía y Competitividad’ for a predoctoral FPI grant.
21
22
23
24
25
26
27
28
29
30
31
32
33
34
35

36 **REFERENCES**
37
38

- 39 (1) Zhang, X.; Chi, Z.; Zhang, Y.; Liu, S.; Xu, J., Recent advances in mechanochromic
40 luminescent metal complexes. *J. Mater. Chem. C* **2013**, 1, 3376-3390.
41 (2) Luo, X.; Li, J.; Li, C.; Heng, L.; Dong, Y. Q.; Liu, Z.; Bo, Z.; Tang, B. Z., Reversible
42 Switching of the Emission of Diphenyldibenzofulvenes by Thermal and Mechanical Stimuli.
43 *Adv. Mater.* **2011**, 23, 3261-3265.
44 (3) Ni, J.; Zhang, X.; Qiu, N.; Wu, Y.-H.; Zhang, L.-Y.; Zhang, J.; Chen, Z.-N.,
45 Mechanochromic Luminescence Switch of Platinum(II) Complexes with 5-
46 Trimethylsilylethynyl-2,2'-bipyridine. *Inorg. Chem.* **2011**, 50, 9090-9096.
47 (4) Zhang, X.; Wang, J.-Y.; Ni, J.; Zhang, L.-Y.; Chen, Z.-N., Vapochromic and
48 Mechanochromic Phosphorescence Materials Based on a Platinum(II) Complex with 4-
49 Trifluoromethylphenylacetylide. *Inorg. Chem.* **2012**, 51, 5569-5579.
50 (5) Shan, G.-G.; Li, H.-B.; Zhu, D.-X.; Su, Z.-M.; Liao, Y., Intramolecular [small pi]-stacking in
51 cationic iridium(iii) complexes with a triazole-pyridine type ancillary ligand: synthesis,
52 photophysics, electrochemistry properties and piezochromic behavior. *J. Mater. Chem.* **2012**, 22,
53 12736-12744.
54
55
56
57
58
59
60

- 1
2
3
4
5
6
7
8
9
10
11
12
13
14
15
16
17
18
19
20
21
22
23
24
25
26
27
28
29
30
31
32
33
34
35
36
37
38
39
40
41
42
43
44
45
46
47
48
49
50
51
52
53
54
55
56
57
58
59
60
- (6) Sagara, Y.; Mutai, T.; Yoshikawa, I.; Araki, K., Material Design for Piezochromic Luminescence: Hydrogen-Bond-Directed Assemblies of a Pyrene Derivative. *J. Am. Chem. Soc.* **2007**, 129, 1520-1521.
- (7) Kunzelman, J.; Kinami, M.; Crenshaw, B. R.; Protasiewicz, J. D.; Weder, C., Oligo(p-phenylene vinylene)s as a “New” Class of Piezochromic Fluorophores. *Adv. Mater.* **2008**, 20, 119-122.
- (8) Chung, J. W.; You, Y.; Huh, H. S.; An, B.-K.; Yoon, S.-J.; Kim, S. H.; Lee, S. W.; Park, S. Y., Shear- and UV-Induced Fluorescence Switching in Stilbenic π -Dimer Crystals Powered by Reversible [2 + 2] Cycloaddition. *J. Am. Chem. Soc.* **2009**, 131, 8163-8172.
- (9) Sagara, Y.; Kato, T., Stimuli-Responsive Luminescent Liquid Crystals: Change of Photoluminescent Colors Triggered by a Shear-Induced Phase Transition. *Angew. Chem., Int. Ed.* **2008**, 47, 5175-5178.
- (10) Irie, M.; Fukaminato, T.; Sasaki, T.; Tamai, N.; Kawai, T., Organic chemistry: A digital fluorescent molecular photoswitch. *Nature* **2002**, 420, 759-760.
- (11) Kishimura, A.; Yamashita, T.; Yamaguchi, K.; Aida, T., Rewritable phosphorescent paper by the control of competing kinetic and thermodynamic self-assembling events. *Nat Mater* **2005**, 4, 546-549.
- (12) Mutai, T.; Satou, H.; Araki, K., Reproducible on-off switching of solid-state luminescence by controlling molecular packing through heat-mode interconversion. *Nat Mater* **2005**, 4, 685-687.
- (13) Sagara, Y.; Kato, T., Mechanically induced luminescence changes in molecular assemblies. *Nat. Chem.* **2009**, 1, 605-610.
- (14) Hou, X.; Ke, C.; Bruns, C. J.; McGonigal, P. R.; Pettman, R. B.; Stoddart, J. F., Tunable solid-state fluorescent materials for supramolecular encryption. *Nat. Commun.* **2015**, 6.
- (15) Ito, H.; Muromoto, M.; Kurenuma, S.; Ishizaka, S.; Kitamura, N.; Sato, H.; Seki, T., Mechanical stimulation and solid seeding trigger single-crystal-to-single-crystal molecular domino transformations. *Nat. Commun.* **2013**, 4.
- (16) Yagai, S.; Okamura, S.; Nakano, Y.; Yamauchi, M.; Kishikawa, K.; Karatsu, T.; Kitamura, A.; Ueno, A.; Kuzuhara, D.; Yamada, H.; Seki, T.; Ito, H., Design amphiphilic dipolar π -systems for stimuli-responsive luminescent materials using metastable states. *Nat. Commun.* **2014**, 5.
- (17) Ning, Z.; Chen, Z.; Zhang, Q.; Yan, Y.; Qian, S.; Cao, Y.; Tian, H., Aggregation-induced Emission (AIE)-active Starburst Triarylamine Fluorophores as Potential Non-doped Red Emitters for Organic Light-emitting Diodes and Cl₂ Gas Chemodosimeter. *Advanced Functional Materials* **2007**, 17, 3799-3807.
- (18) Kinami, M.; Crenshaw, B. R.; Weder, C., Polyesters with Built-in Threshold Temperature and Deformation Sensors. *Chem. Mater.* **2006**, 18, 946-955.
- (19) Toal, S. J.; Jones, K. A.; Magde, D.; Trogler, W. C., Luminescent Silole Nanoparticles as Chemoselective Sensors for Cr(VI). *J. Am. Chem. Soc.* **2005**, 127, 11661-11665.
- (20) Hirata, S.; Watanabe, T., Reversible Thermoresponsive Recording of Fluorescent Images (TRF). *Adv. Mater.* **2006**, 18, 2725-2729.
- (21) Lim, S.-J.; An, B.-K.; Jung, S. D.; Chung, M.-A.; Park, S. Y., Photoswitchable Organic Nanoparticles and a Polymer Film Employing Multifunctional Molecules with Enhanced Fluorescence Emission and Bistable Photochromism. *Angew. Chem., Int. Ed.* **2004**, 43, 6346-6350.

- 1
2
3 (22) Chi, Y.; Chou, P.-T., Transition-metal phosphors with cyclometalating ligands:
4 fundamentals and applications. *Chem. Soc. Rev.* **2010**, 39, 638-655.
5
6 (23) Dixon, I. M.; Collin, J.-P.; Sauvage, J.-P.; Flamigni, L.; Encinas, S.; Barigelletti, F., A
7 family of luminescent coordination compounds: iridium() polyimine complexes. *Chem. Soc. Rev.*
8 **2000**, 29, 385-391.
9
10 (24) Flamigni, L.; Barbieri, A.; Sabatini, C.; Ventura, B.; Barigelletti, F., Photochemistry and
11 Photophysics of Coordination Compounds: Iridium. In *Photochemistry and Photophysics of*
12 *Coordination Compounds II*, Balzani, V.; Campagna, S., Eds. Springer Berlin Heidelberg: 2007;
13 Vol. 281, pp 143-203.
14
15 (25) Wong, W.-Y.; Ho, C.-L., Functional metallophosphors for effective charge carrier
16 injection/transport: new robust OLED materials with emerging applications. *J. Mater. Chem.*
17 **2009**, 19, 4457-4482.
18
19 (26) Williams, J. A. G.; Wilkinson, A. J.; Whittle, V. L., Light-emitting iridium complexes
20 with tridentate ligands. *Dalton Trans.* **2008**, 2081-2099.
21
22 (27) You, Y.; Park, S. Y., Phosphorescent iridium(III) complexes: toward high
23 phosphorescence quantum efficiency through ligand control. *Dalton Trans.* **2009**, 1267-1282.
24
25 (28) Wong, W.-Y.; Ho, C.-L., Heavy metal organometallic electrophosphors derived from
26 multi-component chromophores. *Coord. Chem. Rev.* **2009**, 253, 1709-1758.
27
28 (29) Ulbricht, C.; Beyer, B.; Friebe, C.; Winter, A.; Schubert, U. S., Recent Developments in
29 the Application of Phosphorescent Iridium(III) Complex Systems. *Adv. Mater.* **2009**, 21, 4418-
30 4441.
31
32 (30) Sasabe, H.; Kido, J., Multifunctional Materials in High-Performance OLEDs: Challenges
33 for Solid-State Lighting. *Chem. Mater.* **2011**, 23, 621-630.
34
35 (31) You, Y.; Nam, W., Photofunctional triplet excited states of cyclometalated Ir(III)
36 complexes: beyond electroluminescence. *Chem. Soc. Rev.* **2012**, 41, 7061-7084.
37
38 (32) Lamansky, S.; Djurovich, P.; Murphy, D.; Abdel-Razzaq, F.; Kwong, R.; Tsyba, I.;
39 Bortz, M.; Mui, B.; Bau, R.; Thompson, M. E., Synthesis and Characterization of
40 Phosphorescent Cyclometalated Iridium Complexes. *Inorg. Chem.* **2001**, 40, 1704-1711.
41
42 (33) Tamayo, A. B.; Alleyne, B. D.; Djurovich, P. I.; Lamansky, S.; Tsyba, I.; Ho, N. N.; Bau,
43 R.; Thompson, M. E., Synthesis and Characterization of Facial and Meridional Tris-
44 cyclometalated Iridium(III) Complexes. *J. Am. Chem. Soc.* **2003**, 125, 7377-7387.
45
46 (34) Lowry, M. S.; Hudson, W. R.; Pascal, R. A.; Bernhard, S., Accelerated Luminophore
47 Discovery through Combinatorial Synthesis. *J. Am. Chem. Soc.* **2004**, 126, 14129-14135.
48
49 (35) Baldo, M. A.; O'Brien, D. F.; You, Y.; Shoustikov, A.; Sibley, S.; Thompson, M. E.;
50 Forrest, S. R., Highly efficient phosphorescent emission from organic electroluminescent
51 devices. *Nature* **1998**, 395, 151-154.
52
53 (36) Hong, Y.; Lam, J. W. Y.; Tang, B. Z., Aggregation-induced emission: phenomenon,
54 mechanism and applications. *Chem. Commun.* **2009**, 4332-4353.
55
56 (37) Mei, J.; Hong, Y.; Lam, J. W. Y.; Qin, A.; Tang, Y.; Tang, B. Z., Aggregation-Induced
57 Emission: The Whole Is More Brilliant than the Parts. *Adv. Mater.* **2014**, 26, 5429-5479.
58
59 (38) Luo, J.; Xie, Z.; Lam, J. W. Y.; Cheng, L.; Chen, H.; Qiu, C.; Kwok, H. S.; Zhan, X.;
60 Liu, Y.; Zhu, D.; Tang, B. Z., Aggregation-induced emission of 1-methyl-1,2,3,4,5-
pentaphenylsilole. *Chem. Commun.* **2001**, 1740-1741.
(39) You, Y.; Huh, H. S.; Kim, K. S.; Lee, S. W.; Kim, D.; Park, S. Y., Comment on
'aggregation-induced phosphorescent emission (AIPE) of iridium(III) complexes': origin of the
enhanced phosphorescence. *Chem. Commun.* **2008**, 3998-4000.

- 1
2
3 (40) Zhao, Q.; Li, L.; Li, F.; Yu, M.; Liu, Z.; Yi, T.; Huang, C., Aggregation-induced
4 phosphorescent emission (AIPE) of iridium(III) complexes. *Chem. Commun.* **2008**, 685-687.
- 5 (41) Huang, K.; Wu, H.; Shi, M.; Li, F.; Yi, T.; Huang, C., Reply to comment on 'aggregation-
6 induced phosphorescent emission (AIPE) of iridium(III) complexes': origin of the enhanced
7 phosphorescence. *Chem. Commun.* **2009**, 1243-1245.
- 8 (42) Shan, G.-G.; Zhu, D.-X.; Li, H.-B.; Li, P.; Su, Z.-M.; Liao, Y., Creation of cationic
9 iridium(III) complexes with aggregation-induced phosphorescent emission (AIPE) properties by
10 increasing rotation groups on carbazole peripheries. *Dalton Trans.* **2011**, 40, 2947-2953.
- 11 (43) Shan, G.-G.; Li, H.-B.; Cao, H.-T.; Zhu, D.-X.; Li, P.; Su, Z.-M.; Liao, Y., Reversible
12 piezochromic behavior of two new cationic iridium(III) complexes. *Chem. Commun.* **2012**, 48,
13 2000-2002.
- 14 (44) Chen, Y.; Qiao, L.; Yu, B.; Li, G.; Liu, C.; Ji, L.; Chao, H., Mitochondria-specific
15 phosphorescent imaging and tracking in living cells with an AIPE-active iridium(III) complex.
16 *Chem. Commun.* **2013**, 49, 11095-11097.
- 17 (45) Shan, G.-G.; Li, H.-B.; Sun, H.-Z.; Zhu, D.-X.; Cao, H.-T.; Su, Z.-M., Controllable
18 synthesis of iridium(III)-based aggregation-induced emission and/or piezochromic luminescence
19 phosphors by simply adjusting the substitution on ancillary ligands. *J. Mater. Chem. C* **2013**, 1,
20 1440-1449.
- 21 (46) Wu, Y.; Sun, H.-Z.; Cao, H.-T.; Li, H.-B.; Shan, G.-G.; Duan, Y.-A.; Geng, Y.; Su, Z.-
22 M.; Liao, Y., Stepwise modulation of the electron-donating strength of ancillary ligands:
23 understanding the AIE mechanism of cationic iridium(III) complexes. *Chem. Commun.* **2014**, 50,
24 10986-10989.
- 25 (47) Wu, H.; Yang, T.; Zhao, Q.; Zhou, J.; Li, C.; Li, F., A cyclometalated iridium(III)
26 complex with enhanced phosphorescence emission in the solid state (EPESS): synthesis,
27 characterization and its application in bioimaging. *Dalton Trans.* **2011**, 40, 1969-1976.
- 28 (48) Howarth, A. J.; Patia, R.; Davies, D. L.; Lelj, F.; Wolf, M. O.; Singh, K., Elucidating the
29 Origin of Enhanced Phosphorescence Emission in the Solid State (EPESS) in Cyclometallated
30 Iridium Complexes. *European Journal of Inorganic Chemistry* **2014**, 2014, 3657-3664.
- 31 (49) Quartapelle Procopio, E.; Mauro, M.; Panigati, M.; Donghi, D.; Mercandelli, P.; Sironi,
32 A.; D'Alfonso, G.; De Cola, L., Highly Emitting Concomitant Polymorphic Crystals of a
33 Dinuclear Rhenium Complex. *J. Am. Chem. Soc.* **2010**, 132, 14397-14399.
- 34 (50) Leung, N. L. C.; Xie, N.; Yuan, W.; Liu, Y.; Wu, Q.; Peng, Q.; Miao, Q.; Lam, J. W. Y.;
35 Tang, B. Z., Restriction of Intramolecular Motions: The General Mechanism behind
36 Aggregation-Induced Emission. *Chem. Eur. J.* **2014**, 20, 15349-15353.
- 37 (51) Garg, K.; Ganapathi, E.; Rajakannu, P.; Ravikanth, M., Stereochemical modulation of
38 emission behaviour in E/Z isomers of diphenyldipyrroethene from aggregation induced emission
39 to crystallization induced emission. *Phys. Chem. Chem. Phys.* **2015**, 17, 19465-19473.
- 40 (52) Choi, S.; Bouffard, J.; Kim, Y., Aggregation-induced emission enhancement of a meso-
41 trifluoromethyl BODIPY via J-aggregation. *Chem. Sci.* **2014**, 5, 751-755.
- 42 (53) Hu, R.; Lager, E.; Aguilar-Aguilar, A.; Liu, J.; Lam, J. W. Y.; Sung, H. H. Y.; Williams,
43 I. D.; Zhong, Y.; Wong, K. S.; Peña-Cabrera, E.; Tang, B. Z., Twisted Intramolecular Charge
44 Transfer and Aggregation-Induced Emission of BODIPY Derivatives. *J. Phys. Chem. C* **2009**,
45 113, 15845-15853.
- 46 (54) Hu, R.; Li, S.; Zeng, Y.; Chen, J.; Wang, S.; Li, Y.; Yang, G., Understanding the
47 aggregation induced emission enhancement for a compound with excited state intramolecular
48 proton transfer character. *Phys. Chem. Chem. Phys.* **2011**, 13, 2044-2051.
- 49
50
51
52
53
54
55
56
57
58
59
60

- 1
2
3
4
5
6
7
8
9
10
11
12
13
14
15
16
17
18
19
20
21
22
23
24
25
26
27
28
29
30
31
32
33
34
35
36
37
38
39
40
41
42
43
44
45
46
47
48
49
50
51
52
53
54
55
56
57
58
59
60
- (55) Lei, Y.; Liu, Y.; Guo, Y.; Chen, J.; Huang, X.; Gao, W.; Qian, L.; Wu, H.; Liu, M.; Cheng, Y., Multi-Stimulus-Responsive Fluorescent Properties of Donor- π -Acceptor Indene-1,3-dionemethylene-1,4-dihydropyridine Derivatives. *J. Phys. Chem. C* **2015**, 119, 23138-23148.
- (56) Cho, D. W., Excimer and exciplex emissions of 1,8-naphthalimides caused by aggregation in extremely polar or nonpolar solvents. *New J. Chem.* **2014**, 38, 2233-2236.
- (57) Alam, P.; Kaur, G.; Sarmah, A.; Roy, R. K.; Choudhury, A. R.; Laskar, I. R., Highly Selective Detection of H⁺ and OH⁻ with a Single-Emissive Iridium(III) Complex: A Mild Approach to Conversion of Non-AIEE to AIEE Complex. *Organometallics* **2015**, 34, 4480-4490.
- (58) Alam, P.; Kaur, G.; Kachwal, V.; Gupta, A.; Roy Choudhury, A.; Laskar, I. R., Highly sensitive explosive sensing by "aggregation induced phosphorescence" active cyclometalated iridium(iii) complexes. *J. Mater. Chem. C* **2015**, 3, 5450-5456.
- (59) Alam, P.; Kaur, G.; Chakraborty, S.; Roy Choudhury, A.; Laskar, I. R., "Aggregation induced phosphorescence" active "rollover" iridium(iii) complex as a multi-stimuli-responsive luminescence material. *Dalton Trans.* **2015**, 44, 6581-6592.
- (60) Alam, P.; Kaur, G.; Climent, C.; Pasha, S.; Casanova, D.; Alemany, P.; Roy Choudhury, A.; Laskar, I. R., New 'aggregation induced emission (AIE)' active cyclometalated iridium(iii) based phosphorescent sensors: high sensitivity for mercury(ii) ions. *Dalton Trans.* **2014**, 43, 16431-16440.
- (61) Alam, P.; Das, P.; Climent, C.; Karanam, M.; Casanova, D.; Choudhury, A. R.; Alemany, P.; Jana, N. R.; Laskar, I. R., Facile tuning of the aggregation-induced emission wavelength in a common framework of a cyclometalated iridium(iii) complex: micellar encapsulated probe in cellular imaging. *J. Mater. Chem. C* **2014**, 2, 5615-5628.
- (62) Butschke, B.; Schwarz, H., "Rollover" cyclometalation - early history, recent developments, mechanistic insights and application aspects. *Chem. Sci.* **2012**, 3, 308-326.
- (63) Dong, Y. Q.; Lam, J. W. Y.; Tang, B. Z., Mechanochromic Luminescence of Aggregation-Induced Emission Luminogens. *J. Phys. Chem. Lett.* **2015**, 6, 3429-3436.
- (64) Chi, Z.; Zhang, X.; Xu, B.; Zhou, X.; Ma, C.; Zhang, Y.; Liu, S.; Xu, J., Recent advances in organic mechanofluorochromic materials. *Chem. Soc. Rev.* **2012**, 41, 3878-3896.
- (65) Ma, Z.; Wang, Z.; Teng, M.; Xu, Z.; Jia, X., Mechanically Induced Multicolor Change of Luminescent Materials. *ChemPhysChem* **2015**, 16, 1811-1828.
- (66) Z., J. X., Z. Chi., ed.; Mechanochromic Fluorescent Materials: Phenomena, Materials and Applications; Eds.; Royal Society of Chemistry: London, 2014.
- (67) Todres, Z. V., Recent advances in the study of mechanochromic transitions of organic compounds. *Journal of Chemical Research* **2004**, 2004, 89-93.
- (68) Alexander, B. D.; Johnson, B. J.; Johnson, S. M.; Casalnuovo, A. L.; Pignolet, L. H., Mixed transition metal-gold cluster hydrides. *J. Am. Chem. Soc.* **1986**, 108, 4409-4417.
- (69) Alexander, B. D.; Johnson, B. J.; Johnson, S. M.; Boyle, P. D.; Kann, N. C.; Mueting, A. M.; Pignolet, L. H., Heterobimetallic gold-iridium, silver-iridium, and gold-ruthenium bis(μ -hydrido) complexes. X-ray crystal and molecular structures of [AuRu(H)₂(dppm)₂(PPh₃)]PF₆ and [Ir(H)₂(bpy)(PPh₃)₂]PF₆. *Inorg. Chem.* **1987**, 26, 3506-3513.
- (70) Kizaki, T.; Matsumoto, T.; Ogo, S., Dissolved N₂ sensing by pH-dependent Ru complexes. *Dalton Trans.* **2010**, 39, 1339-1344.
- (71) Cabon, Y.; Kleijn, H.; Siegler, M. A.; Spek, A. L.; Gebbink, R. J. M. K.; Deelman, B.-J., Dichlorostannylene complexes of group 10 metals, a unique bonding mode stabilized by bridging 2-pyridyldiphenylphosphine ligands. *Dalton Trans.* **2010**, 39, 2423-2427.

- (72) Gong, Y.; Andrews, L.; Liebov, B. K.; Fang, Z.; Garner, I. I. I. E. B.; Dixon, D. A., Reactions of laser-ablated U atoms with (CN)₂: infrared spectra and electronic structure calculations of UNC, U(NC)₂, and U(NC)₄ in solid argon. *Chem. Commun.* **2015**, 51, 3899-3902.
- (73) *CrystalClear 2.0, Rigaku Corporation, Tokyo, Japan 2016.*
- (74) Sheldrick, G., A short history of SHELX. *Acta Crystallographica Section A* **2008**, 64, 112-122.
- (75) Dolomanov, O. V.; Bourhis, L. J.; Gildea, R. J.; Howard, J. A. K.; Puschmann, H., OLEX2: a complete structure solution, refinement and analysis program. *Journal of Applied Crystallography* **2009**, 42, 339-341.
- (76) Frisch, M. J.; Trucks, G. W.; Schlegel, H. B.; Scuseria, G. E.; Robb, M. A.; Cheeseman, J. R.; Scalmani, G.; Barone, V.; Mennucci, B.; Petersson, G. A.; Nakatsuji, H.; Caricato, M.; Li, X.; Hratchian, H. P.; Izmaylov, A. F.; Bloino, J.; Zheng, G.; Sonnenberg, J. L.; Hada, M.; Ehara, M.; Toyota, K.; Fukuda, R.; Hasegawa, J.; Ishida, M.; Nakajima, T.; Honda, Y.; Kitao, O.; Nakai, H.; Vreven, T.; Montgomery Jr., J. A.; Peralta, J. E.; Ogliaro, F.; Bearpark, M. J.; Heyd, J.; Brothers, E. N.; Kudin, K. N.; Staroverov, V. N.; Kobayashi, R.; Normand, J.; Raghavachari, K.; Rendell, A. P.; Burant, J. C.; Iyengar, S. S.; Tomasi, J.; Cossi, M.; Rega, N.; Millam, N. J.; Klene, M.; Knox, J. E.; Cross, J. B.; Bakken, V.; Adamo, C.; Jaramillo, J.; Gomperts, R.; Stratmann, R. E.; Yazyev, O.; Austin, A. J.; Cammi, R.; Pomelli, C.; Ochterski, J. W.; Martin, R. L.; Morokuma, K.; Zakrzewski, V. G.; Voth, G. A.; Salvador, P.; Dannenberg, J. J.; Dapprich, S.; Daniels, A. D.; Farkas, Ö.; Foresman, J. B.; Ortiz, J. V.; Cioslowski, J.; Fox, D. J. *Gaussian 09*, Gaussian, Inc.: Wallingford, CT, USA, 2009.
- (77) Lee, C.; Yang, W.; Parr, R. G., Development of the Colle-Salvetti correlation-energy formula into a functional of the electron density. *Physical Review B* **1988**, 37, 785-789.
- (78) Becke, A. D., Density-functional thermochemistry. III. The role of exact exchange. *The Journal of Chemical Physics* **1993**, 98, 5648-5652.
- (79) Hay, P. J.; Wadt, W. R., Ab initio effective core potentials for molecular calculations. Potentials for K to Au including the outermost core orbitals. *The Journal of Chemical Physics* **1985**, 82, 299-310.
- (80) T. A. Albright; J. K. Burdett; Whangbo, M.-H., *John Wiley & Sons, Ltd, New York 1985.*
- (81) Jayabharathi, J.; Thanikachalam, V.; Sathishkumar, R., Highly phosphorescent green emitting iridium(III) complexes for application in OLEDs. *New J. Chem.* **2015**, 39, 235-245.
- (82) Schanda, J., CIE Colorimetry. In *Colorimetry*, John Wiley & Sons, Inc.: 2007; pp 25-78.
- (83) Dirac, P. A. M., The Quantum Theory of the Emission and Absorption of Radiation. *Proc. Roy. Soc.* **1927**, A114, 243-265.
- (84) Fermi, E., *Nuclear Physics*, University of Chicago Press, Chicago **1950.**
- (85) Bixon, M.; Jortner, J., *Electron Transfer-from Isolated Molecules to Biomolecules, Part 1, Advances in Chemical Physics*, John Wiley & Sons, Inc, New York **1999**, 106.
- (86) Jortner, J., Spiers Memorial Lecture On Dynamics From isolated molecules to biomolecules. *Faraday Discussions* **1997**, 108, 1-22.
- (87) Kodama, Y.; Nishihata, K.; Nishio, M.; Nakagawa, N., Attractive interaction between aliphatic and aromatic systems. *Tetrahedron Lett.* **1977**, 18, 2105-2108.
- (88) M. Nishio; M. Hirota; Y. Umezawa, *The CH/π interaction*, Wiley-VCH, New York, **1998.**

1
2
3 (89) Janiak, C., A critical account on π - π stacking in metal complexes with
4 aromatic nitrogen-containing ligands. *Journal of the Chemical Society, Dalton Transactions*
5 **2000**, 3885-3896.

6
7 (90) Alvarez, S., A cartography of the van der Waals territories. *Dalton Trans.* **2013**, 42,
8 8617-8636.

9 (91) Sun, H.; Liu, S.; Lin, W.; Zhang, K. Y.; Lv, W.; Huang, X.; Huo, F.; Yang, H.; Jenkins,
10 G.; Zhao, Q.; Huang, W., Smart responsive phosphorescent materials for data recording and
11 security protection. *Nat. Commun.* **2014**, 5.
12
13
14
15
16
17
18
19
20
21
22
23
24
25
26
27
28
29
30
31
32
33
34
35
36
37
38
39
40
41
42
43
44
45
46
47
48
49
50
51
52
53
54
55
56
57
58
59
60

Exploring the Origin of ‘Aggregation Induced Emission’ Activity and ‘Crystallization Induced Emission’ in Organometallic Iridium(III) Cationic Complexes: Influence of Counterions

Parvej Alam^{a†}, Clàudia Climent^{b†}, Gurpreet Kaur^c, David Casanova^{d,e}, Angshuman Roy Choudhury^e, Ashish Gupta^f, Pere Alemany^{*b}, Inamur Rahaman Laskar^{*a}

The emission colour of solid state samples of a new cationic iridium(III) complex exhibiting ‘aggregation induced emission (AIE)’ activity, crystallization induced emission is found to vary in crystals with different counteranions. Analysis of the crystal packing, the frontier molecular orbitals and the characterization of the relevant low-lying excited states by means of time dependent density functional theory suggests the restriction of internal motion (RIM) as the most plausible origin of the observed AIE effect in these crystals.

